Water movement through plant roots
Exact solutions of the water flow equation in roots with linear or exponential piecewise hydraulic properties

Meunier Félicien[1], Couvreur Valentin[2], Draye Xavier[2], Zarebanadkouki Mohsen[3], Vanderborght Jan[4,5], and Javaux Mathieu[1,4]

[1]Earth and Life Institute-Environment, Université catholique de Louvain, Louvain-la-Neuve, Belgium
[2]Earth and Life Institute-Agronomy, Université catholique de Louvain, Louvain-la-Neuve, Belgium
[3]Department of Plant Ecology, Bayreuth University, Bayreuth, Germany
[4]Forschungszentrum Juelich GmbH, Agrosphere (IBG-3), Juelich, Germany
[5]Division of Soil and Water Management, KU Leuven, Leuven, Belgium

Correspondence to: Félicien Meunier (felicien.meunier@uclouvain.be)

Abstract. In 1978, Landsberg and Fowkes presented a solution of the water flow equation inside a root with uniform hydraulic properties. These properties are root radial conductivity and axial conductance, which control, respectively, the radial water flow between the root surface and xylem and the axial flow within the xylem. From the solution for the xylem water potential, functions that describe the radial and axial flow along the root axis were derived. These solutions can also be used to derive root macroscopic parameters that are potential input parameters of hydrological and crop models. In this paper, novel analytical solutions of the water flow equation are developed for roots whose hydraulic properties vary along their axis, which is the case for most plants. We derived solutions for single roots with linear or exponential variations of hydraulic properties with distance to root tip. These solutions were subsequently combined to construct single roots with complex hydraulic property profiles. The analytical solutions allow one to verify numerical solutions and to get a generalization of the hydric behaviour with the main influencing parameters of the solutions. The resulting flow distributions in heterogeneous roots differed from those in uniform roots and simulations led to more regular, less abrupt variations of xylem suction or radial flux along root axes. The model could successfully be applied to maize effective root conductance measurements to derive radial and axial hydraulic properties. We also show that very contrasted root water uptake patterns arise when using either uniform or heterogeneous root hydraulic properties in a soil-root model. Optimal root radius that maximizes water uptake under a carbon cost constraint was also studied. The optimal radius was shown to be highly dependent on the root hydraulic properties and close to observed ones in maize roots. We finally used the obtained functions for evaluating the impact of root maturation *versus* root growth on water uptake. Very diverse uptake strategies arise from the analysis. These solutions open new avenues to investigate for optimal genotype x environment x management interactions by optimization, for example, of plant-scale macroscopic hydraulic parameters used in ecohydrogolocial models.

1 Introduction

Global crop production is negatively affected by drought that is the most significant stress in agriculture (Cattivelli et al., 2008). Drought stress can be defined as the plant's inability to take up and transport the required amount of water to the shoot, leading to stomatal closure and reduced yield (Campos et al., 2004). Transferring water from the soil to the shoot, thus preventing leaves from dehydration, is a major role of the vascular root systems (McElrone et al., 2013). Root water uptake (RWU) is driven by water potential gradients between soil and atmosphere and is mainly controlled by stomatal regulation, plant hydraulic resistance and soil water availability (Volpe et al., 2013). Both root system architecture and hydraulics are key for the location and intensity of water uptake (Leitner et al., 2014). These properties are encapsulated in the concept of root system hydraulic architecture (Lobet et al., 2014). Under high transpiration demand, from the root-soil interface to the evaporative sites, water crosses first radially the root tissues towards the root xylem vessels and then flows up to the leaves (Passioura, 1980). The tissues' ability to transfer the water radially is called hydraulic radial conductivity while the capacity to conduct water axially is the axial conductance or xylem conductance.

Measurements of root hydraulic properties demonstrated that radial conductivity and axial conductance both change with root tissue maturation for a given plant genotype (Frensch and Steudle, 1989a; Doussan et al., 1998b; Zwieniecki et al., 2002). The root anatomy and disposition of cell layers on water pathways impact root radial conductivity (Steudle, 2000). The development of endodermal and exodermal apoplastic barriers, first with a Casparian band, then with suberin lamellae and lignified tertiary walls constitutes major hydraulic impedances to water flow (Enstone et al., 2002). Aquaporins also play a central role in root radial conductivity by facilitating water flow across cell membranes (Chaumont and Tyerman, 2014) and their location and expression change with the maturation of apoplastic barriers (Hachez et al., 2006). Besides, root axial conductance increases with abundance, shape and size of xylem vessels, increasing from apical regions with protoxylem to basal regions with late metaxylem vessels (McCully and Canny, 1988). These maturation steps make younger (distal) root regions more functional for water uptake, while mature (proximal) regions are more adapted to water axial transfer, as confirmed by water flow measurements of Sanderson (1983) in barley or Zarebanadkouki et al. (2016) in lupine. Uniform root hydraulic properties would on the contrary concentrate water uptake on the proximal region (Landsberg and Fowkes, 1978). Figure 1 (top) summarizes estimates and measurements of root radial conductivity and axial conductance of primary maize roots as a function of distance to root tip (Frensch and Steudle, 1989b; Frensch et al., 1996; Zwieniecki et al., 2002; Doussan et al., 1998b; Bramley et al., 2007). Figure 1 (bottom panels) also illustrates the changes of primary root anatomy with distance to tip as observed by Steudle and Peterson (1998) with root cross sections. With an inverse modelling approach coupled to tracer data from Varney and Canny (1993), Doussan et al. (1998b) produced an extensive estimation of root hydraulic property profiles with piecewise functions for both maize primary and lateral roots. The hydraulic conductivity profiles of Zwieniecki et al. (2002) comes as well from an inverse modelling exercise (Meunier et al., 2017).

Despite these evidences that uniform root properties are more the exception than the rule, today a majority of models assume explicitly (Biondini, 2008; Roose and Schnepf, 2008) or implicitly (Zhuang et al., 2001) that roots have homogenous properties. For instance, most crop and hydrological models assume that root water uptake is proportional to root length density, implicitly

assuming uniform root radial properties and non-limiting xylem conductances while numerical models already showed that the arrangement of root hdyraulic properties dramatically affects dynamics and efficiency of water uptake (Bechmann et al., 2014). It is important to realise that assuming uniform root properties will not only impact the root water uptake and water potential distributions, but also the effective root conductance, when up-scaled to the full plant (Couvreur et al., 2012). Today, there is

5   no easy way to predict how root property distribution impacts these plant scale properties.

An analytical solution for root water uptake and flow was developed by Landsberg and Fowkes (1978) but only for uniform roots. Ariyaratna (1990) extended later the analytical solution for a linear increase of the radial conductivity. Besides this study, no general analytical solution of the root water flow equation is presently available.
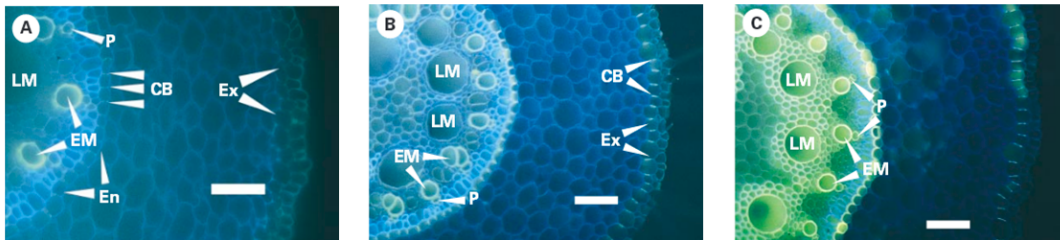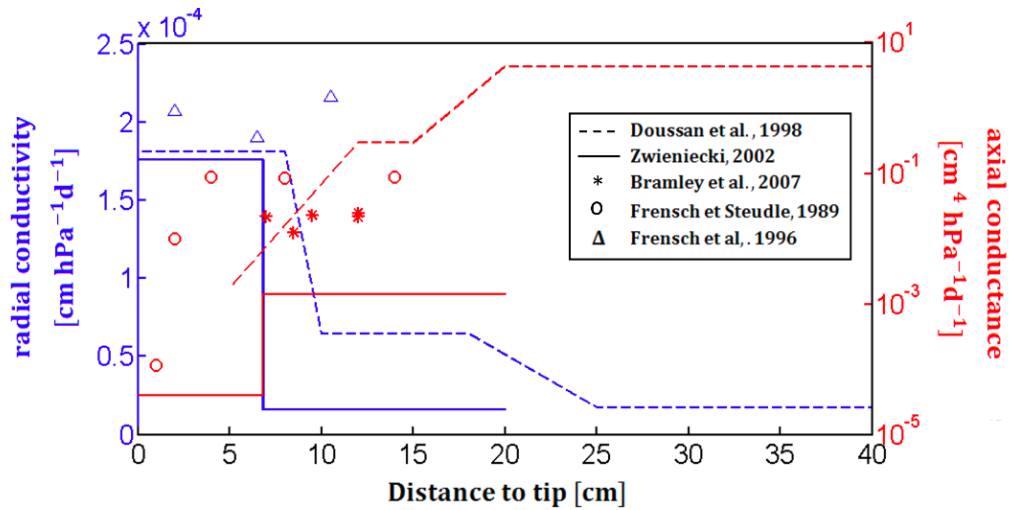
Figure 1. Top: Maize radial conductivity (left axis) and axial conductance (right axis) of primary roots as measured in several studies. Bottom: maize primary root cross-sections obtained at different development stages. The root cross-sections are the work of Steudle and Peterson (1998). The scale bars are 100 microns long. Ex = exodermis, En = endodermis, CB = casparian band, P = protoxylem, EM = early metaxylem, LM = late metaxylem. (a) Immature Ex, En with CB, mature P, mature EM and immature LM, (b) mature Ex, En with asymmetrically thickened walls, mature P and EM, immature LM (c) similar to (b) with mature LM. Reproduced by courtesy of Steudle and Peterson.

On the other hand, solving the water flow equation in the root system can also be achieved using finite difference for any

10   root hydraulic property distribution (Alm et al., 1992) and for any root system architecture (Doussan et al., 1998a). Typically

the water flow equation in the root system is solved by segmenting root system into small root parts called root segments. Water potentials within the structure are discrete so that each segment has (i) an unique xylem water potential connected to contiguous segment xylem potentials by axial conductances, and (ii) a soil-root interface water potential connected to the segment xylem potential by a radial conductance. Analogically to Ohm's law, radial and axial rates of water flow in each

5   segment are proportional to the associated water potential differences. The water flow equations are solved for the generated root system hydraulic architecture by inverting a conductance matrix of the root system network (Doussan et al., 1998a; Javaux et al., 2008). If root segments were divided into smaller sub-segments though, water potentials and flows would slightly vary in each segment. The result is consequently an approximation of the exact solution that would be obtained for root segments of infinitesimal length. Developing analytical solutions would allow the community to verify numerical models' accuracy for

10   heterogeneous roots.

      In this paper we show that uniform root property assumption may be relaxed and yet analytical solutions of the water flow equation in roots are within our reach. Our objective is to present novel mathematical solutions of the water flow equation in roots with non-uniform radial and axial hydraulic properties closer to reality and more efficient than current existing models. We also developed solutions for growing roots at given elongation rates, which make the uptake distribution time-dependent. This

15   widens the solution of Landsberg and Fowkes (1978) to roots growing at rates potentially decoupled from tissue maturation rate. These solutions can be used for numerical model benchmarking or, as it was done here, to derive root hydraulic properties from effective conductance measurements and to assess the impact of hydraulic traits on root water uptake patterns. Eventually, we also develop an up-scaled model to predict how heterogeneous root hydraulic properties impact effective root conductance and water uptake distribution and their evolution with time.

2 Theory

2.1 Water flow equation in a single root

In the following, we only consider single root, i.e. without laterals. Consequently we sometimes use simply the word roots for single roots. When used, the terms root stretch or root segment designate a portion of a single root characterized by specific root properties.

Assuming that root water content does not fluctuate, water mass balance in infinitesimal root segments of a cylindrical root of radius $r\,[\mathrm{L}]$ and total length $l\,[\mathrm{L}]$ under uniform soil-root interface water potential yields (Landsberg and Fowkes, 1978):

$$\frac{dJ_x(z)}{dz} = -2\pi r k_r(z)\left(\Psi_x(z) - \Psi_{soil}\right) \tag{1}$$

where $J_x\,[\mathrm{L}^3\mathrm{T}^{-1}]$ is the axial flow of water within the xylem in the root, $k_r\,[\mathrm{LT}^{-1}\mathrm{P}^{-1}]$ is the root radial conductivity, $\Psi_x\,[\mathrm{P}]$ is the xylem water potential, $\Psi_{soil}\,[\mathrm{P}]$ is the uniform water potential at soil-root interface, and $z\,[\mathrm{L}]$ is the distance from the root tip along the root axis. We use the abbreviations L, T and P for length, time and pressure unit dimensions, respectively. The axis z is always chosen parallel to the root axis. Note that the right-hand side term corresponds to root radial flow rate per unit root length $q_r\,[\mathrm{L}^2\mathrm{T}^{-1}]$:

$$q_r = -2\pi r k_r(z)\left(\Psi_x(z) - \Psi_{soil}\right) \tag{2}$$

Axial flow is driven by the water potential gradient in the xylem vessels:

$$J_x(z) = -k_x(z)\frac{d\Psi_x(z)}{dz} \tag{3}$$

with $k_x\,[\mathrm{L}^4\mathrm{T}^{-1}\mathrm{P}^{-1}]$ the axial conductance of the root. Combining Eq. (1) and (3), we obtain:

$$\frac{d}{dz}\left(k_x(z)\frac{d\Psi_x(z)}{dz}\right) = 2\pi r k_r(z)\left(\Psi_x(z) - \Psi_{soil}\right) \tag{4}$$

which is the general equation of water flow equation in roots.

2.2 General solutions of root water flow

The differential Eq. (4) can be solved for various distributions of root properties and boundary conditions. Since Eq. (4) is a second-order differential equation, its general solution is of the form:

$$\Psi_x(z) = \Psi_{soil} + c_{1,i}f_{1,i}(z) + c_{2,i}f_{2,i}(z) \tag{5}$$

Where $c_{1,i}$ and $c_{2,i}$ are constants whose values depend on root hydraulic properties and boundary conditions at root's ends and $f_{1,i}$ and $f_{2,i}$ are differentiable functions of z whose type depends on the root hydraulic property profiles. The subscript i as it will be further explained is used to distinguish root stretches. It can vary between 1 and N, the total number of stretches in the single root. The length between the root apex and a root stretch proximal part is called l_i. When $i = N$, $l_i = l$.

5 For simple functions $k_x(z)$ and $k_r(z)$ (i.e. constant, linear and exponential), analytical expressions for $f_1(z)$ and $f_2(z)$, $c_{1,i}$ and $c_{2,i}$ are derived in Appendix A. However, $k_x(z)$ and $k_r(z)$ profiles along a root generally correspond to piecewise collections of these simple functions (see for example (Doussan et al., 1998b)). Hence, we establish a procedure to compute analytical expressions of water flow in a single root with segments connected in series with contrasted hydraulic property profiles. Figure 2 presents a sketch of a single root made of five stretches delimited by dashed vertical lines.

10 Deriving the coefficients $c_{1,i}$ and $c_{2,i}$ in any root stretch i requires boundary conditions at the limits of each stretch (i.e., at $z = l_{i-1}$, the root stretch i's distal end and at $z = l_i$, its proximal end). The bottom flux boundary condition at the distal end of stretch i is called $J_{i-1}\,[\mathrm{L^3T^{-1}}]$, and the xylem water potential at the proximal end of stretch i is $\Psi_{proximal,i}\,[\mathrm{P}]$ as it appears in Fig. 2 and as stated in Eq. (6):

$$
\begin{cases}
J_x(l_{i-1}) = J_{i-1} \\
\Psi_x(l_i) = \Psi_{proximal,i}
\end{cases}
\tag{6}
$$

15 Note that $J_0 = 0$ (no axial flow at the root tip), and $\Psi_{proximal,N} = \Psi_{collar}$ (the xylem water potential at the proximal end of the last root stretch N is the plant collar potential).
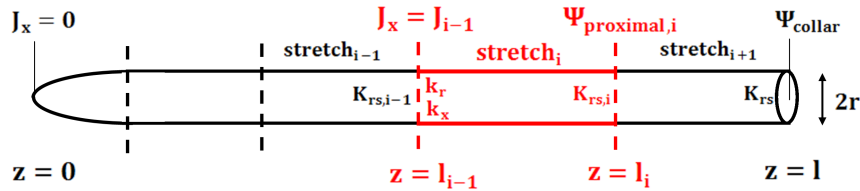
Figure 2. Single root made of five stretches (the dashed vertical lines are stretch boundaries). For root stretch i, boundary condition at $z = l_{i-1}$ (distal end) is the water flow J_{i-1} and at $z = l_i$ (proximal end) the xylem water potential $\Psi_{proximal,i}$. For details, see text.

2.3 Derivation of macroscopic root hydraulic properties

Only J_0 and $\Psi_{proximal,N}$ are predefined root boundary conditions and none of the root stretches has both boundary conditions known (J_{i-1} and $\Psi_{proximal,i}$) so the solution of the water flow equation is not straightforward unless the root is made of a

20 single stretch. To solve this problem, the concept of root macroscopic parameters is used.

The root macroscopic parameters consist in the root system effective conductance $K_{rs}\,[\mathrm{L^3T^{-1}P^{-1}}]$ and the Standard Uptake Density $SUD\,[\mathrm{L^{-1}}]$ (Couvreur et al., 2012; Meunier et al., 2017). These parameters are used in soil-root water transfer models

that stem from principles of water flow in root hydraulic architecture but do not rely on an explicit geometrical description of root system (Couvreur et al., 2012). In contrast to Couvreur, Meunier et al. (2017) revisited these definitions and applied them to any root or part of a root system. They are calculated in homogeneous soil conditions and are defined here as function of the root length l_i as:

$$
5 \quad \begin{cases} K_{rs,i} = \frac{J_x(l_i)}{\Psi_{soil} - \Psi_x(l_i)} \\ SUD_i(z) = \frac{q_r(z)}{J_x(l_i)} \end{cases} \tag{7}
$$

These macroscopic parameters are always independent of the boundary conditions (Ψ_{soil} and Ψ_{collar}): they only depend on root geometric (radius and length) and hydraulic properties ($k_r(z)$ and $k_x(z)$). Let us note that the $K_{rs,i}$ and SUD_i as defined in Eq. (7) represent the root macroscopic parameters after addition of i stretches ignoring thus the root stretches after the considered zone. The terms K_{rs} and SUD are used instead of $K_{rs,N}$ and SUD_N, respectively, and correspond to the
10 macroscopic parameters of the entire root:

$$
\begin{cases} K_{rs} = \frac{J_x(l)}{\Psi_{soil} - \Psi_x(l)} \\ SUD(z) = \frac{q_r(z)}{J_x(l)} \end{cases} \tag{8}
$$

The macroscopic parameters may be calculated by a recursive equation (see Appendix B for demonstration):

$$
\begin{cases} K_{rs,i} = k_x(l_i) \frac{\left(-K_{rs,i-1}f_{2,i}(l_{i-1}) + f'_{2,i}(l_{i-1})k_x(l_{i-1})\right)f'_{1,i}(l_i) + \left(K_{rs,i-1}f_{1,i}(l_{i-1}) - f'_{1,i}(l_{i-1})k_x(l_{i-1})\right)f'_{2,i}(l_i)}{K_{rs,i-1}f_{1,i}(l_{i-1})f_{2,i}(l_i) - K_{rs,i-1}f_{1,i}(l_i)f_{2,i}(l_{i-1}) - f'_{1,i}(l_{i-1})f_{2,i}(l_i)k_x(l_{i-1}) + f_{1,i}(l_i)f'_{2,i}(l_{i-1})k_x(l_{i-1})} \\ SUD_i(z) = \frac{2\pi r k_r(z)}{k_x(l_i)} \frac{\left(-K_{rs,i-1}f_{2,i}(l_{i-1}) + f'_{2,i}(l_{i-1})k_x(l_{i-1})\right)f_{1,i}(z) + \left(K_{rs,i-1}f_{1,i}(l_{i-1}) - f'_{1,i}(l_{i-1})k_x(l_{i-1})\right)f_{2,i}(z)}{\left(-K_{rs,i-1}f_{2,i}(l_{i-1}) + f'_{2,i}(l_{i-1})k_x(l_{i-1})\right)f'_{1,i}(l_i) + \left(K_{rs,i-1}f_{1,i}(l_{i-1}) - f'_{1,i}(l_{i-1})k_x(l_{i-1})\right)f'_{2,i}(l_i)} \end{cases} \tag{9}
$$

where Lagrange notation is used for derivative. The recursive formulation is useful to solve the water flow equation when
15 dealing with multiple-stretched roots. We start, in such a case, with the calculation of $K_{rs,1}$ (i.e., the effective conductance of the most distal stretch) using Eq. (9) (with $K_{rs,0} = 0$ because the axial flow is null at root apex). The obtained $K_{rs,1}$ is then used as $K_{rs,i-1}$ to calculate the effective conductance of the distal part from the second stretch $K_{rs,2}$ using Eq. (9). This procedure is then used again to derive the $K_{rs,i}$ of all stretches until the root collar is reached. The obtained set of $K_{rs,i}$'s or $K_{rs,i-1}$'s are then used to calculate the coefficients $c_{1,i}$ and $c_{2,i}$ for the different stretches using:

$$
20 \quad \begin{cases} c_{1,i} = \frac{(\Psi_{proximal,i} - \Psi_{soil})\left(-K_{rs,i-1}f_{2,i}(l_{i-1}) + f'_{2,i}(l_{i-1})k_x(l_{i-1})\right)}{K_{rs,i-1}f_{1,i}(l_{i-1})f_{2,i}(l_i) - K_{rs,i-1}f_{1,i}(l_i)f_{2,i}(l_{i-1}) - f'_{1,i}(l_{i-1})f_{2,i}(l_i)k_x(l_{i-1}) + f_{1,i}(l_i)f'_{2,i}(l_{i-1})k_x(l_{i-1})} \\ c_{2,i} = \frac{(\Psi_{proximal,i-1} - \Psi_{soil})\left(K_{rs,i-1}f_{1,i}(l_{i-1}) - f'_{1,i}(l_{i-1})k_x(l_{i-1})\right)}{K_{rs,i-1}f_{1,i}(l_{i-1})f_{2,i}(l_i) - K_{rs,i-1}f_{1,i}(l_i)f_{2,i}(l_{i-1}) - f'_{1,i}(l_{i-1})f_{2,i}(l_i)k_x(l_{i-1}) + f_{1,i}(l_i)f'_{2,i}(l_{i-1})k_x(l_{i-1})} \end{cases} \tag{10}
$$

as demonstrated in Appendix B. Since in Eq. (10), only the potential at the proximal part of the stretch is needed as a boundary condition (in addition to the distal effective root conductance), the calculation starts at the proximal end of the root system where the root collar potential Ψ_{collar} is known. The obtained $c_{1,i}$ and $c_{2,i}$ for the proximal stretch are subsequently

used in Eq. (5) to calculate the water potential at the distal part of the stretch. The water potential is then used to calculate the coefficients of the next stretch (towards the root tip). This procedure is used until the most distal stretch is reached. As SUD depends on the collar water flow, it can not be calculated for each zone. However it can be derived at the end of the procedure when the xylem water potential is defined everywhere inside the root and when the effective root conductance has been already calculated.

2.4 Resolution of the root water flow equation

We here analyse six cases of hydraulic conductance variations along a root axis: the uniform root (already developed by Landsberg and Fowkes (1978)), a single root with linear root hydraulic property profiles and a single root with exponential root hydraulic property profiles. For the two latter cases, the radial conductivity and the axial conductance may change alone or simultaneously. Table 1 summarizes the six cases with the corresponding local hydraulic properties. Note that the linear increase of axial conductance was already studied by Ariyaratna (1990). Table 2 summarizes the solutions of the root water flow equation obtained for the six considered cases. The resolution details are provided in Appendix A.

The parameters used in Table 1 are gathered as well as their units in Table 3 (two first columns). To simplify the solutions of the root water flow equation, some parameters are combined. The definition of combined parameters is also given in Table 3 with their corresponding units (two last columns).

These functions can be combined in complex root with several root stretches with Eq. (9), (10) and the entire root boundary conditions: Ψ_{collar} and $J_0 = 0$.

Figure 3 shows the procedure to solve the water flow problem in a root with variable hydraulic properties. First we need to know whether the root is made of one or several stretches. Then we have to determine the coefficients $c_{1,i}$ and $c_{2,i}$ for each single zone, $i \in [1\ N]$ by determining the type of root stretch we deal with and by using Eq. (10). Thanks to these coefficients, we obtain the effective root conductance after addition of each stretch by applying Eq. (9). Finally we calculate the xylem potential, the axial flow, the radial flow per root length and the macroscopic parameters using the appropriate equations and analytical functions given in Table 2. The corresponding equations are mentioned in the figure.

If the root is made of only one stretch, there is no need to calculate intermediary effective root conductances. The solutions of Table 2 are then used with the no flux boundary condition coefficients to obtain the macroscopic parameters as well as the water xylem potential radial and axial water flow profiles along the root axis. This particular case is analysed in Appendix C.

2.5 Properties of an ageing root

The water flow equation resolution derived in the previous sections was obtained for a root of a specific length. In the next sections, we show how to modify the solution when the root is growing and developing.
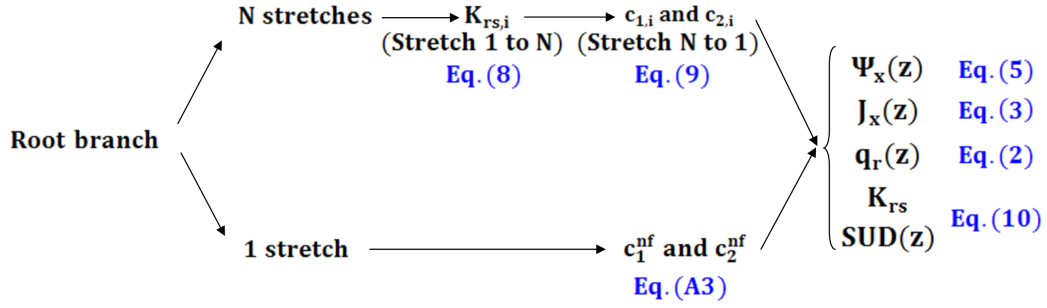
Figure 3. Flowchart of the water flow equation resolution in roots with heterogeneous hydraulic properties

2.5.1 Root growth

In this section we introduce the root elongation. As in many studies, the properties are measured as a function of emerging time instead of distance to tip, we provide here a tool to switch from one to another. Basically an equation of the root elongation rate is required. We consider here an instantaneous growth rate $v(t)\,\mathrm{LT}^{-1}]$, function of the actual time $t\,[\mathrm{T}]$, given by:

$$v(t) = v_0 exp\left(\frac{-v_0}{l_{max}}t\right) \tag{11}$$

where $v_0\,[\mathrm{LT}^{-1}]$ is the initial elongation rate and $l_{max}\,[\mathrm{L}]$ is the root maximal length (Pagès et al., 2004). Note that if $l_{max}\,[\mathrm{L}]$ is large enough, then the elongation rate is almost constant and equals v_0. When the transition ages (i.e. root ages at which root hydraulic property change), $age_i\,[\mathrm{T}]$, are known, the stretch lengths, $stretch_i(t)\,[\mathrm{L}]$ are given by:

$$stretch_i(t) = \begin{cases} 0, t < age_i \\ l_{max}\left(1 - exp\left(\frac{-v_0}{l_{max}}(t - age_i)\right)\right), t \geq age_i \text{ and } t \leq age_{i+1} \\ l_{max}\left(exp\left(-\frac{v_0}{l_{max}}(t - age_{i+1})\right) - exp\left(-\frac{v_0}{l_{max}}(t - age_i)\right)\right), t > age_{i+1} \end{cases} \tag{12}$$

See Appendix D for details.

2.5.2 Root development

When roots get older, their macroscopic hydraulic parameters vary not only because they grow but also because of root tissue maturation. Maturation is defined here as an evolution of root hydraulic properties as a function of root age (and not of distance to root tip as done in the previous sections). This process is modelled by introducing root hydraulic properties depending on root age, such as:

$$\begin{cases} k_r = k_{r0}exp(-mt) \\ k_x = k_{x0}exp(mt) \end{cases} \tag{13}$$

where $m\,[\mathrm{T}^{-1}]$ is the maturation rate. These equations are similar to the ones used in the exponential root hydraulic properties subsection (see Sect. A3) except that they define the properties as a function of time instead of distance to tip. Other root development rate can be imagined, similar to the other functions developed in the previous sections.

3 Model illustration

In this section, we highlight the potential of the new functions with a modelling exercise. We start with simple theoretical illustrations of the model. We then explain how pressure probe measurements can be used with modelling to derive local hydraulic properties. These results are then inserted first in a soil-root model to test the uptake efficiency of a heterogeneous root as compared to a uniform one, and then in an optimization algorithm to assess an optimal radius of the analysed roots. Finally we show how root *vs* development rates can reveal very contrasted uptake strategies. Another added value of analytical solutions is their potential use to verify the current numerical solution. One example is given in Appendix E.

3.1 Comparison between uniform and heterogeneous roots

3.1.1 Roots with the same effective conductance

First, three theoretical roots were simulated. Figure 4 represents how the radial conductivity (a) and the axial conductance (b) depend on distance to tip for these three roots. The blue solid lines represent a root with constant hydraulic properties while the dashed and dotted are roots with linear and exponential hydraulic property profiles (radially and axially), respectively. The numerical values are chosen so that the effective conductance K_{rs} of the three roots is rigorously the same.
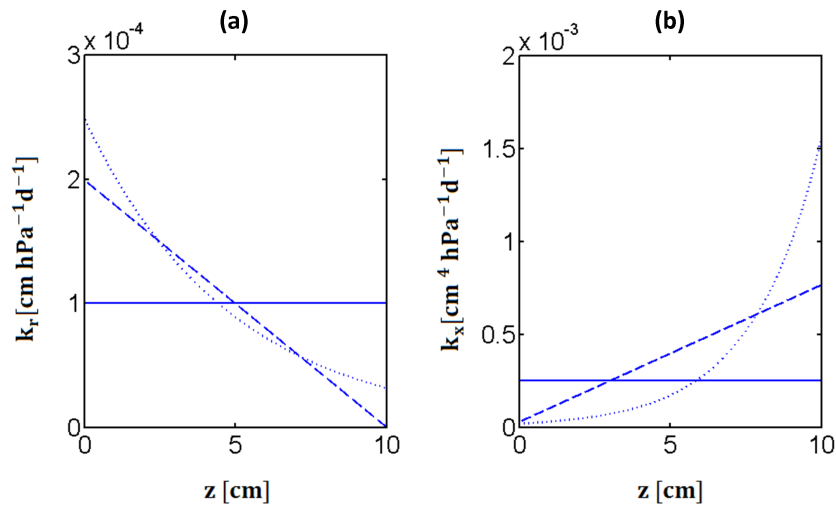
Figure 4. Variation with distance to root tip of radial conductivity (a) and axial conductance (b) along a single root with constant hydraulic properties (solid blue line), a single root with linear hydraulic profiles (dashed lines) and a single root with exponential hydraulic profiles (dotted lines). The origin of the z-axis is at the root tip.

The water flow equation is then solved for these three roots and the xylem potential as well as the radial and axial flow are computed to assess their divergences. Xylem water potential is obtained thanks to Eq. (A1) for the uniform root, (A4) for the linearly changing root and (A5) for the exponentially varying root. The calculations were performed for a constant Ψ_{collar} of

-2000 hPa and a uniform soil water potential of 0 hPa. Radial flow per root length q_r and axial water flow J_x are obtained applying Eq. (2) and Eq. (3), respectively, to the three different cases.

We also define two root parameters combining root hydraulic and geometric properties:

$$
\begin{cases}
\tau(z) = \sqrt{\frac{2\pi r k_r(z)}{k_x(z)}} \\
\kappa(z) = \sqrt{2\pi r k_r(z) k_x(z)}
\end{cases}
$$

5  The units of these root parameters are $[\mathrm{L}^{-1}]$ and $[\mathrm{L}^{-3}\mathrm{P}^{-1}\mathrm{T}^{-1}]$, respectively. These parameters have the same definitions than in the case of the uniform root (see Appendix A.1) but they depend now on the position along the root axis. τ indicates how fast the root system conductance changes and how homogeneous the water uptake along the root axis under homogeneous soil conditions is. κ is an indicator of the maximal possible root system conductance.

3.1.2 Water flow in a maize lateral root

10 Here, we compare single roots with complex hydraulic profiles (as they have been observed) and constant root hydraulic properties in terms of distribution of water xylem potential, radial and axial flows and macroscopic parameters. Lateral maize root properties from Doussan et al. (1998b) are analysed here. This constitutes an illustration of the multiple-stretched single root. In their study, they described axial conductance and radial conductivity as stepwise functions of the root age or distance to tip. They justified it by the root tissue maturation and development. We converted the transition ages to distance to tip

15 transition position as explained in the previous section. We considered a constant elongation rate of 1 cm per day. Three other root hydraulic property uniform functions were also tested: minimal, maximal and mean values of observed profiles for both hydraulic properties. Whether constant root hydraulic properties could mimic more complex situations is consequently investigated comparing the different scenarios in terms of uptake, flow and macroscopic parameters with a constant Ψ_{collar} of -2000 hPa.

20 ### 3.2 Inverse modeling of root hydraulic properties

A root pressure probe was used to measure root effective conductance as well as axial conductance of unbranched brace maize roots. To do so, nine maize were grown in aluminium containers filled with silty soil. When plants were seven weeks old, the containers were opened, roots were carefully washed from the soil and selected maize brace roots were excised from the stem. They were then connected to a pressure probe in order to derive their hydraulic properties in an experiment similar to

25 the one first presented by Frensch and Steudle (1989a). We only give the general idea here. For more details, we refer to the explanations of Frensch and Steudle (1989a).

  Unbranched intact roots were around 35 cm long when first connected to the root pressure probe. A series of pressure steps were carried out (3-5 steps) to induce a flow of water into the root after a stable value of root pressure was reached, which took between 30 to 120 min. Increments of 20 to 50kPa were used for successive pressure clamps. Pressure was held constant at

30 each increment for 10 to 120 s. The distance that metal rode (meniscus) inside the capillary had moved was used to calculate

the water volume and as a consequence the flow rate by dividing by the duration of the step. The linear regression of flow rate plotted against the applied pressure difference led to the effective root conductance for this specific length. The root was then cut towards its tip and reconnected to the root pressure probe to repeat the measurement until the root end was reached.

Axial hydraulic conductance was determined after cutting the root connected to the root pressure probe with a razor blade at a distance of 2 cm from its proximal end. Similar to the measurement of effective conductance, a series of pressure clamps were carried out to induce water flow into the small root segment. The local axial conductance was calculated as the product of the segment length by the slope of the linear regression of flow rate plotted against the applied pressure difference.

The profile of axial conductance was first fitted using piecewise functions. Both axial conductances absolute values and positions of the transition were optimized. When obtained, further optimization was required to derive the profile of radial conductivity using the effective root conductance. Several scenarios, including uniform, single- and multi-stretches hydraulic properties, were tested. Since the number of fitting parameters was not constant between scenarios, adjusted coefficient of determination allowed us to discriminate the best scenario. An uniform root (both radially and axially) was also tested to compare the results with the solution of Landsberg and Fowkes (1978). In total six scenarios were considered: uniform radial conductivity and axial conductances alongside with a linear stepwise distribution for the axial conductance (that corresponded to the observations, see results section) combined with five different root radial conductivity distributions. The latter are linear, exponential, 3-stepwise, 2 steps linear piecewise and 3 steps linear piecewise distributions. Together they represent the complete set of solutions that were presented in this study.

3.3 Root in a heterogeneous soil

The uniform and heterogeneous hydraulic profiles that best fitted the measurements of the previous experiments were then tested to compute the macroscopic parameters, K_{rs} and SUD, for any root length. These calculations allowed us to simulate the water flow in the soil-root continuum. To do so, we used the model developed by Couvreur et al. (2012) and Couvreur et al. (2014) that only requires the macroscopic parameters (in terms of root parameters) to predict the water flow from the bulk soil to the root collar. The soil sink term is calculated as the sum of the local radial flow to the root which, in turn, are given by (Meunier et al., 2017)

$$q_r(z) = T_{act}SUD(z) + K_{rs}\left(\Psi_{sr}(z) - \Psi_{seq}\right)SUD(z)$$

with $T_{act}\,[L^3T^{-1}]$ the proximal end water flow, $\Psi_{sr}(z)\,[P]$ the soil-root interface potential and $\Psi_{seq} = \int_0^l SUD(z)\Psi_{sr}(z)dz\,[P]$ the equivalent soil potential. In the simulations, the root were supposed to be vertical in a 3D loamy soil box of 10 x 10 x 30 cm^3 with a constant total water uptake of 1 cm^3d^{-1} and a constant elongation rate of 1 cm (root initial length of 1 cm, final length of 21 cm). When the root collar potential reached $-1.5MPa$, the root top boundary condition was switched from flux to pressure-head. A constant pressure was then maintained as top boundary condition and the total uptake was consequently reduced (Meunier et al., 2016). We here considered root growth to assess how it impacts the sink location and hence the plant water status. The coupling between the root and soil water flow was achieved following Javaux et al. (2008), i.e. the soil water

flow is obtained by solving Richards equation, the soil-root interface potential is the distance-weighted soil root potential and soil and root equations are solved iteratively until convergence. For more details, see Javaux et al. (2008); Couvreur et al. (2012)

3.4 Optimal geometric properties

5   The new solutions of the water flow equation are key to estimate optimal geometric properties of roots. As an illustration we may want to maximize the effective conductance K_{rs} of uniform roots and compare the results with those of roots with varying hydraulic property profiles. Using a carbon cost as a constraint, it writes:

maximize $K_{rs}(r,l)$ subject to $V_0 = \pi r^2 l$

where $V_0 \left[L^3 \right]$ is the volume constraint. To solve this optimization problem, Lagrange multipliers λ are useful. We define a

10   new function L:

$$L(r,l,\lambda) = K_{rs}(r,l) + \lambda \left(\pi r^2 l - V_0 \right)$$

whose maximum is found when:

$$\nabla_{r,l,\lambda} L = 0$$

The previous equation is equivalent to:

$$
\begin{cases}
\frac{\partial K_{rs}}{\partial r} + 2\lambda \pi r l = 0 \\
\frac{\partial K_{rs}}{\partial l} + \lambda \pi r^2 = 0 \\
V_0 = \pi r^2 l
\end{cases}
\tag{14}
$$

Using appropriate equations to calculate the effective conductance, we find an optimal radius and length that maximize root water uptake. As an illustration, we compare the optimal root radius of a root with constant hydraulic properties, a root whose constant root properties depend on the root radius (Biondini, 2008) and a root with heterogeneous root properties as observed in the pressure probe experiment. Mathematically, it writes, respectively:

$$
\begin{cases}
\text{Constant } k_r \text{ and } k_x : k_r(z) = k_{r0} \text{ and } k_x(z) = k_{x0} \\
\text{Uniform } k_r(r) \text{ and } k_x(r) : k_r(r) = k_{r0} \frac{r_0}{r} \text{ and } k_x(r) = b^* r^5 \\
\text{Heterogeneous } k_r \text{ and } k_x : k_r(z) = f(z) \text{ and } k_x(z) = g(z)
\end{cases}
\tag{15}
$$

The parametrization for the heterogeneous root and the uniform root are the best heterogeneous and uniform profiles derived from the pressure probe experiment for brace roots. For the root whose hydraulic properties depend on the root radius, we used the parameters of Biondini (2008) for maize (r_0 [L], k_{r0} [L^{4}P^{-1}T^{-1}] and b^* [L^{-1}P^{-1}T^{-1}]). The constraint volume V_0 was the mean observed volume for the maize brace roots. $f(z)$ and $g(z)$ are observed functions for the radial and axial hydraulic property, respectively.

3.5   Root water uptake strategy

In this last example, we again consider a single growing root whose development and elongation rates can both vary. We varied the root parameters m (development) and $\frac{v_0}{l_{max}}$ (growth) between 0.05 and 0.5 [d^{-1}] and between 0.01 and 0.1 [d^{-1}], respectively to investigate the impact of relative growth and maturation processes on macroscopic parameters and uptake patterns.

4 Results

4.1 Comparison between uniform and heterogeneous roots

4.1.1 Roots with the same effective conductance

Solutions of the water flow equation are shown in Fig. 5 for three different root property distributions (the legend is the same
as in figure 4): uniform, linear and exponential profiles. Xylem water potential is presented in subplot a, the radial flow per root
length in subplot b and the axial water flow in subplot c.
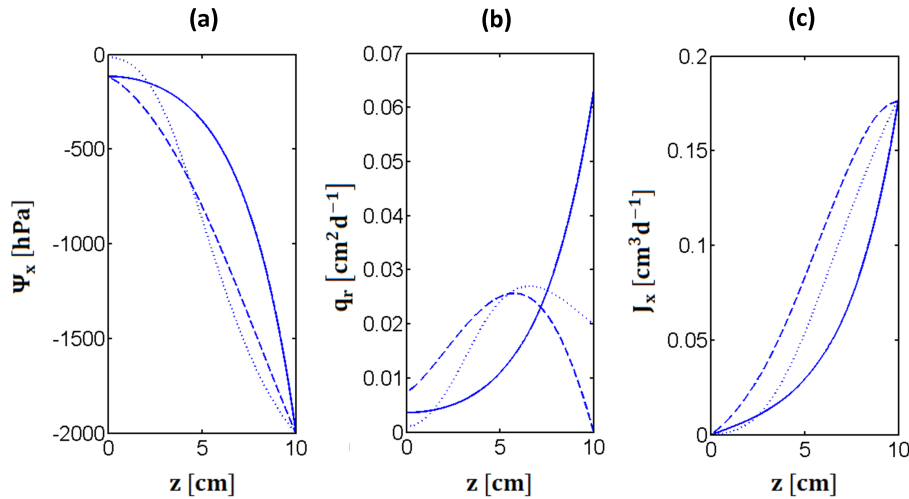
Figure 5. Solutions of the root water flow equation: xylem water potential (a), radial water flow per root length (b) and axial water flow
(c) along a root with constant properties (solid blue line), a root with linear hydraulic profiles (dashed lines) and a root with exponential
hydraulic profiles (dotted lines). The origin of the z-axis is at the root tip.

Even if the collar axial flow is identical for each root (because they have the same effective conductance), their xylem water
potential and root water uptake profiles differ. The potential drop is more homogeneously distributed along the roots with
heterogeneous properties. Furthermore, it is observed that q_r is a monotonic increasing function of distance in the case of the
uniform root, but that the maximal uptake is not located at the root collar anymore for the two other cases. Consequently the
axial flow differ between these three cases.

Root parameters τ and κ are represented in Fig. 6, subplots (a) and (b), respectively. These parameters are constant for a
uniform root. τ is monotonically decreasing for non-uniform roots because the radial conductivity is decreasing and the axial
conductance is increasing along the root axis. The root with linear hydraulic property profiles has a non-monotonic κ while this
parameter is always increasing for roots with exponentially changing hydraulic properties. These hydraulic parameters must be
set in relation with the root macroscopic parameters represented in the bottom line of Fig. 6. In subplot (a) SUD is represented

along the z-axis (note that this subplot is the same as the second subplot of Fig. 5 except that the curve is now normalized so that its integral on total root length is one). K_{rs} is plotted as a function of the root length in subplot (b). It is worth noting that the root system conductances differ very much between these cases. Depending on how k_r and k_x vary along the root, K_{rs} might even decrease with increasing root length (linear root case). This occurs when additional segments with a low k_r

5 are added so that the extra inflow across these segments does not compensate for the extra pressure head loss due to axial flow through these segments. However, when the decrease in k_r with root length levels off while k_x increases still strongly with increasing root length, as it is the case in the exponential scenario, the root system conductance may increase steadily with root length.
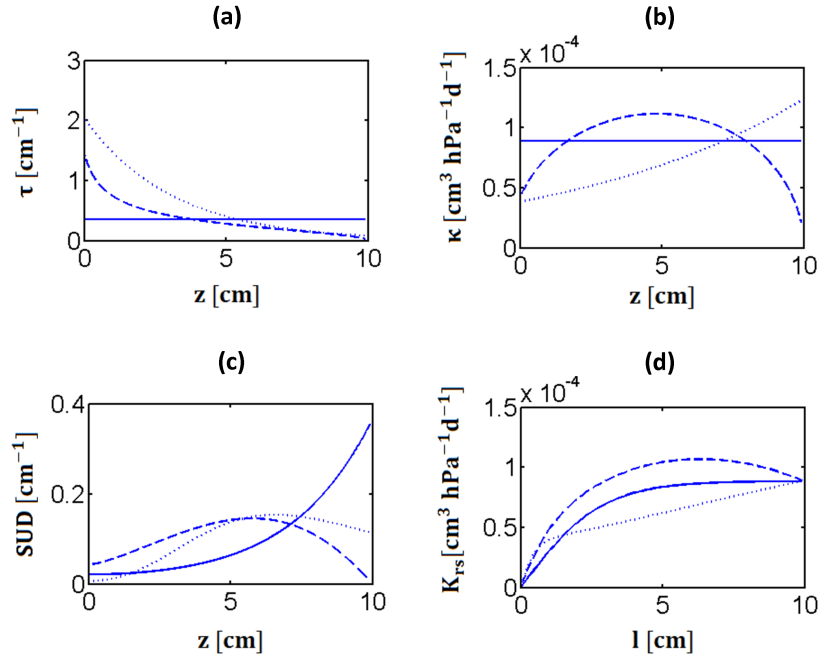
Figure 6. Variation along a single root of root (top line) and macroscopic (bottom line) hydraulic parameters: τ (a), κ (b), SUD (c) and K_{rs} (d) of a single root with constant properties (solid blue line), a single root with linear hydraulic profiles (dashed lines) and a single root with exponential hydraulic profiles (dotted lines).

4.1.2 Water flow in a maize lateral root

10 The local hydraulic property distribution for the lateral roots of maize, as derived by Doussan et al. (1998b), are shown in the two first subplots of Fig. 7 (blue solid lines). These subplots are equivalent to the Fig. 4B of the study of Doussan et al. (1998b) when a constant elongation rate of 1 cm per day is assumed. We removed the isolated distal region (whose axial conductance is null and that consequently does not affect root water fluxes). The red dashed, dotted and dashed-dotted lines correspond to hypothetical roots with uniform properties corresponding to minimal, maximal and mean values of observed hydraulic

properties. When we compare the Doussan distribution of water radial flow per root length and potential with those of constant hydraulic property models (Fig. 7, c and d), we observe that it is not possible to represent its complex behaviour with an apparent/effective uniform model. The drop of water potential is much steeper with heterogeneous than with homogeneous properties (red lines). The decrease in water potential and the increase in axial flow are far more uniform along the composite root than along the homogeneous roots.
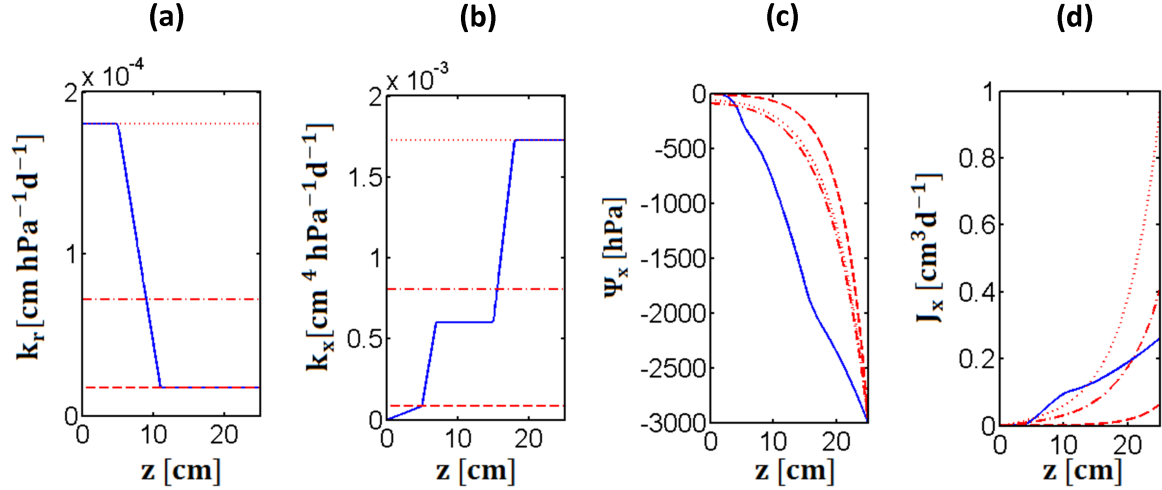
Figure 7. Distributions of radial conductivity (a), axial conductance (b), xylem water potential (c) and axial water flow (d) in a maize lateral root. We used hydraulic properties obtained by Doussan et al. (1998b) (blue solid line) for a maize lateral root or equivalent properties (red lines) with minimal (dashed), maximal (dotted) or mean (dashed-dotted) values. The origin of the z-axis is at the root tip.

We used Eq. (9) to derive the macroscopic parameters of the four roots (the complex root and the three uniform roots). Again both the SUD and the K_{rs} could not be well represented by uniform root properties. It is indeed impossible with these solutions to represent non-monotonic functions as the standard uptake density (subplot (a), Fig. 8) and the effective conductance (subplot (b), Fig. 8). This questions the typical assumptions made by hydrological and crop models, for which the effective conductance is considered proportional to the root length density.

While K_{rs} increases monotonically towards the proximal end for uniform roots, this is no more the case for the heterogeneous root. When considering variations in hydraulic properties along the maize root axis, the analytical solutions that account for these changes revealed considerably different behaviours. The effective conductance even decreases with root length. Similarly with the newly developed solutions, the maximal water uptake location was no more located at root proximal end. Non-monotonic functions of root water uptake emerged from the new solutions.
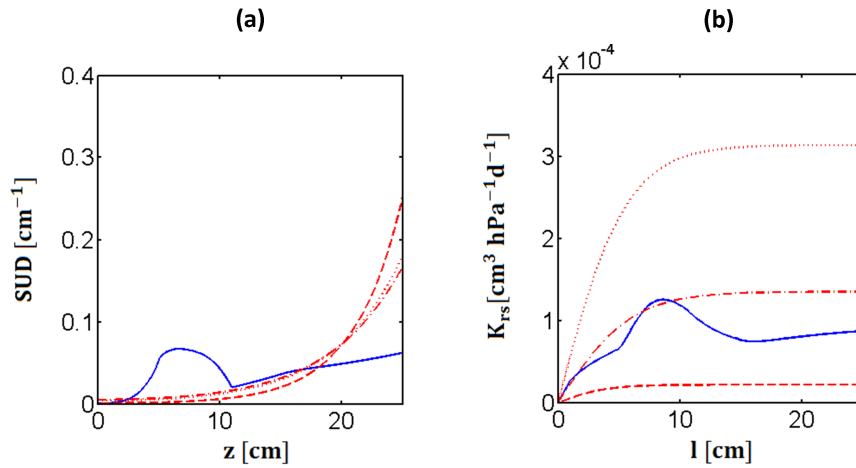
Figure 8. Macroscopic parameters: final SUD (a) and K_{rs} changes (b) for a growing maize lateral root with the local hydraulic properties estimated by Doussan et al. (1998b) (blue solid line) or the equivalent uniform roots (red lines) with minimal (dashed), maximal (dotted) or mean (dashed-dotted) hydraulic property values. The color legend is the same as in the previous figure.

4.2 Inverse modeling of root hydraulic properties

The analytical solutions developed here may serve as well to get local root hydraulic properties distributions along root axes (see below). Here we used experimental measurements of the observed axial and effective conductances as measured by the root pressure probe (represented with black markers in subplots a and d, respectively of Fig. 9). A perfect fit of the xylem
5   conductance profile could be obtained with a linear piecewise function (black dashed line, subplot a). The subplot b reveals the best radial conductivity profiles for some of the tested functions: linear (orange), exponential (yellow), 3-stepwise (mauve), 2 steps linear piecewise (light blue), 3 steps linear piecewise (green). The resulting effective conductance profiles are represented with the same legend in subplot d with contrasting performances (the adjusted coefficients of determination are indicated as well). Note that the y-scales of the subplots are all in log-scale, this explains why the linear stepwise curves are not straight
10   and why the exponential scenario is a straight line. Interestingly the best linear scenario (orange) is the constant function as it also can be seen from subplot b. In subplot c, radial to axial hydraulic properties ratios are plotted as a function of the distance from root tip. The best scenario is the stepwise function for the radial conductivity profile coupled to a piecewise function for the axial conductance profile (mauve scenario). The last scenario that is represented in fig. 9 is an axially and radially uniform root (dark blue). If with such profiles, it is possible to reasonably fit the effective conductance profile (adjusted $r^2 = 0.81$),
15   then, of course, the modelled xylem conductance profile does not fit at all, since high variations were observed between both root extremities.

Clearly it appears that there are different solutions possible for the radial conductivity variations (light blue and mauve are equivalently good). However as shown in subplot b and c, the orders of magnitude of k_r, and as a consequence the radial conductivity to axial conductance ratio, are similar in these best scenarios. It implies that the experiment is sensitive to the
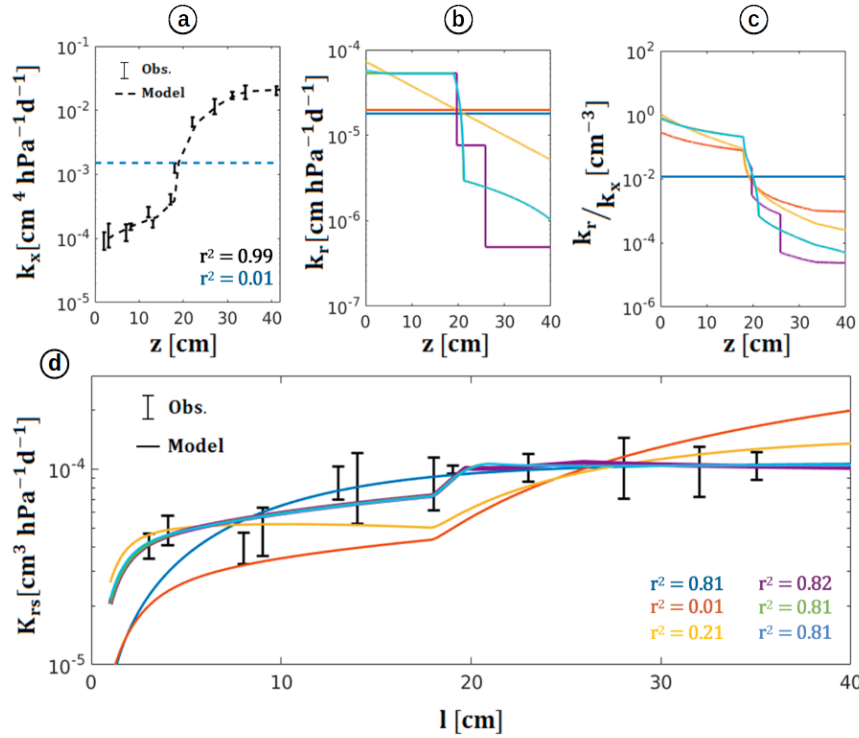
Figure 9. Hydraulic properties of the maize brace roots: axial and effective conductance of different root types as function of distance from root tip (dark symbols, subplots a and d, respectively). Data presented as dots are average of 5 measurements and the error bars represent the standard deviations. In subplot a, two different scenarios were tested: constant (dark blue dashed line) or linear piecewise (black dashedd line) axial conductance. Profiles plotted as solid lines are the best profiles obtained from optimization of root radial conductivity parameters through simulations of water flow into unbranched roots of varying length (subplot d). Subplot b: best fitted profiles of radial conductivity that reproduce measured profiles of effective conductance. Subplot c: ratio of radial conductivity to axial conductance derived from the analysis along the root axis. The best fitted axial conductance profile was used for each scenario except for the uniform root (dark blue).

changes of root radial conductivity even though more knowledge/measurement on local variations of root conductance would be needed to know accurately the root radial conductivity of the brace roots.

The combination of pressure probe experiments with the newly developed solutions of the water flow equation in routine would allow us to derive the local hydraulic properties of roots that are critical for root system water uptake and plant performance (Vadez, 2014).

4.3   Root in a heterogeneous soil

When inserted in a soil-root model, the maize brace uniform root and the one with best scenario of hydraulic properties present contrasted uptake patterns and performances as revealed in fig. 10. Here the roots are growing vertically in a homogeneous soil

to assess the impact of water uptake location on plant water status. In all subplots of this figure, the uniform and heterogeneous roots are represented with dashed and solid lines, respectively. The uniform root decreases its uptake after 6 days because the collar potential reaches the threshold at that time. At the very end of the simulation (20 days), this root had transpired 15% less water than the heterogeneous root, in total. This can be explained by the location of the root water uptake: while the uniform root always takes up water at the top, the heterogeneous root keeps looking for water at its tip. While, as a consequence, the heterogeneous root never feels a too low potential, the top water potential rapidly decreases for the uniform root and critical potential are reached within the xylem vessels that force the root reducing its water uptake. Interestingly for the heterogeneous root both the soil equivalent and collar potentials increase after 5 days because, as the water uptake is mainly located at the root tip in such a case, new wet soil regions are explored by the active root parts (in terms of water uptake) and this impacts the root water status.

The uptake location can be seen from the clipped domain where water velocities at the end of the simulations are shown. A movie of the change in the main water uptake depth is also provided in the supplementary material. While after five days, the xy-averaged soil potentials look similar for both roots, they diverge at the end of the simulation (bottom subplot).
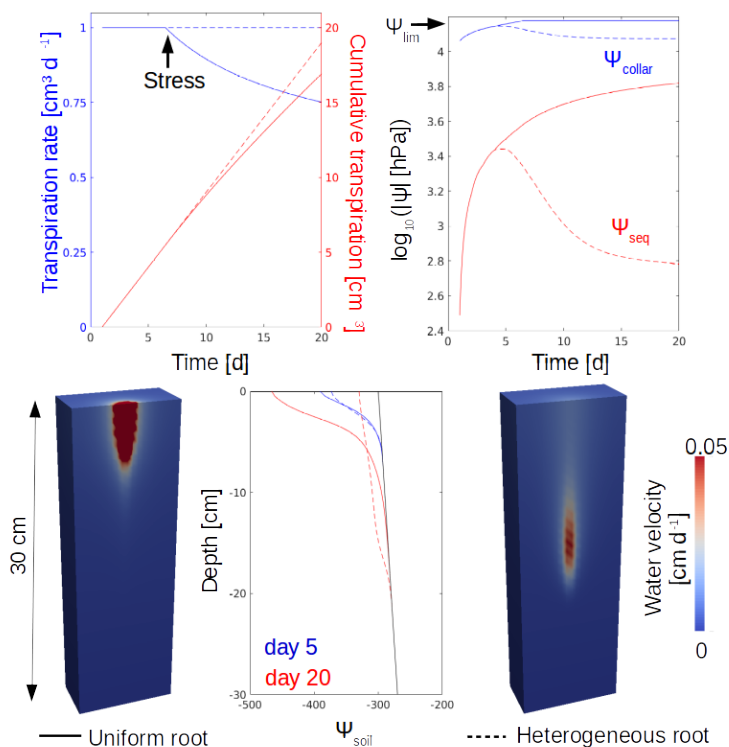
Figure 10. Root perfomances in a coupled soil-root model: changes of instantaneous and cumulative water uptake (top, left) and of collar and equivalent potential (top, right) for an uniform (dashed) and heterogeneous (solid) roots. In the bottom, the z-averaged profiles of soil potentials are plotted early and late in the simulation. The resulting water velocities at the end of the simulation are also shown in the clipped domain for both scenarios.

This simulation underlines how critical the root water uptake location is for the root performance. The environment (that was not changed in the presented simulation) is, of course, important for the overall plant transpiration. The soil hydraulic properties (that redistribute more or less the water) and the climatic demand (that is more or less severe) strongly influence the results. However, we show that the water flow equation solutions, through the macroscopic parameters, can be inserted in water flow models, i.e. in heterogeneous environments to predict how efficient a particular root is.

4.4 Optimal geometric properties

In this section, we look for optimal root traits that would maximize the root water uptake. As an illustration, we compare the effective conductances of a uniform single root, a uniform single root with hydraulic properties varying with its radius, and a single root with exponential hydraulic property profiles. The effective root conductances of the three cases are shown in Fig. 11: the dashed line is the uniform root, the solid line is the uniform root whose hydraulic properties depend on the root radius and the dotted one is the heterogeneous root observed with the pressure probe experiment. The red stars point the optimal radii at which the conductances are maximal for the three scenarios. The black star is the observed pair radius-conductance of maize brace root.
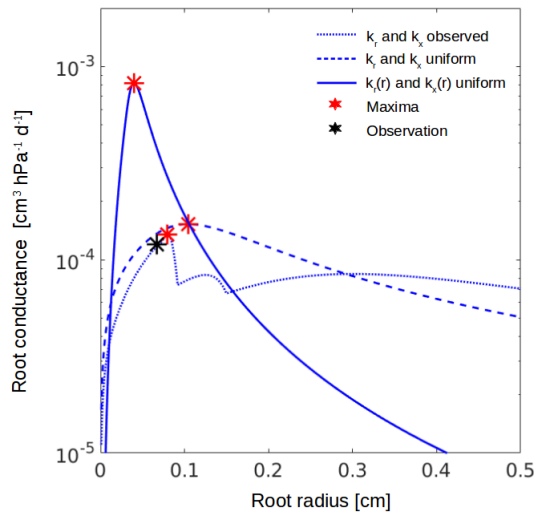
Figure 11. Effective conductance as a function of root radius under a volume constraint for a uniform root whose hydraulic properties depend on the root radius (solid line), a uniform root (dashed line) and a root with observed heterogeneous conductivity profiles (dotted line). The red stars point the optimal radii (i.e., that maximize the effective conductance), the black star the observed one.

Unlike previous approaches (Biondini, 2008; Roose and Schnepf, 2008) we consider here that the hydraulic properties may be functions of the root tissues and do not necessarily depend on the root radius. As highlighted by the red stars, the optimal root radii vary considerably when integrating this concept. We find that optimal root radius is closer with stepwise functions to the observed one than with other conductance variations.

4.5   Root water uptake strategy

Figure 12-a shows the integral of K_{rs} over time when simulating 40 days of growth and maturation of a root whose l_{max} is 10 cm. Four extreme situations are represented: fast growth and slow maturation (case 1), slow growth and maturation (case 2), fast growth and maturation (case 3) and slow growth and fast maturation (case 4), respectively. The effective conductances of these particular roots are plotted as a function of time in Fig. 12-b. They exhibit very contrasted strategies in terms of effective conductance and uptake distributions. When the root growth is fast, the K_{rs} quickly reaches a high value. If the root maturation process is rapid, the final conductance is low. It can also be observed that the root properties change slowly when the root growth is low and rapidly when the root elongation rate is high. Figure 12-c represents the relative $SUD(z)$ (i.e., multiplied by root length) as a function of the relative root position z (i.e., divided by root length) after 20 days of growth. Again contrasted strategies appear with a maximal water uptake location at the root tip for cases 3 and 4 or at the root collar for cases 1 and 2. It is worth noting that a constant elongation rate means a very small elongation rate to maximal root length ratio. So depending on the maturation rate, the constant elongation case rate is similar to case 2 or 4. This illustrates that plants might control their uptake patterns not only by changing their local conductances (Tardieu et al., 2015) but also by adapting their growth rate.
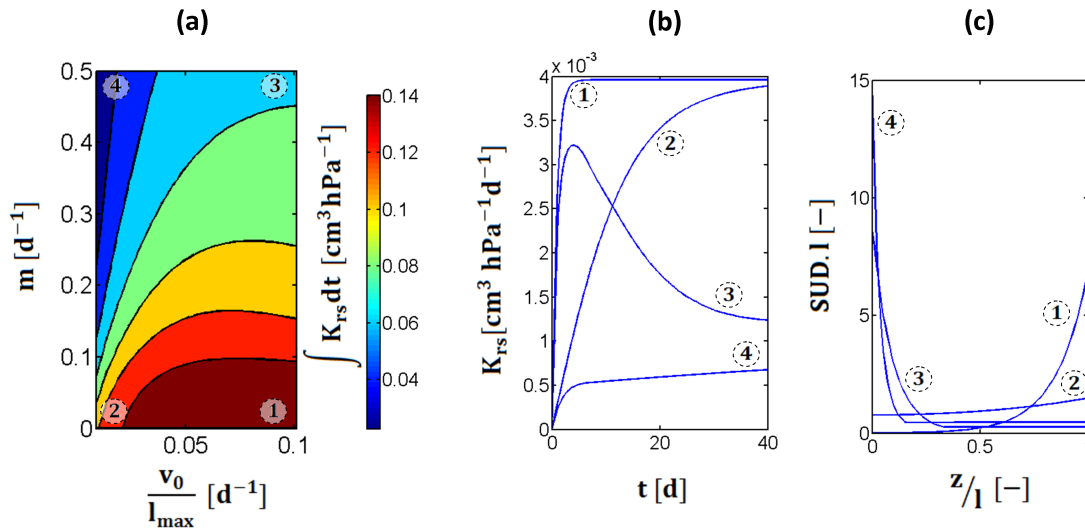
Figure 12. Integral of the effective root conductance over time when changing the elongation rate $\frac{v_0}{l_{max}}$ (x-axis) and the maturation rate m (y-axis) (a). Root hydraulic conductances of the four extreme cases numbered and indicated in (a) as a function of time (b). Relative uptake of the four single roots after 20 days as a function of the relative position to the root tip (l is the root length and $z = 0$ at the tip) (c).

5 Conclusions

Six new solutions of the water flow equation in single roots with different hydraulic property distributions are presented in addition to the uniform hydraulic property solution of Landsberg and Fowkes (1978). These novel solutions account for root hydraulic properties that vary as a function of the distance to root tip. When the radial conductivity and the axial conductance change linearly or exponentially alone or in combination along the root axis, analytical solutions of the xylem potential and water flow inside the root were developed. Explicit equations for macroscopic parameters of the corresponding single roots were derived from these analytical solutions. Moreover, they were associated to make complex single roots of changing root hydraulic property profiles as observed in nature or combined with the root elongation to obtain the root macroscopic parameters and uptake profile as a function of root age, even in heterogeneous soils. These complex functions were not well represented by root of equivalent but constant root hydraulic properties.

This enabled us investigating the effects of root maturation or root tissue development and differentiation on root water uptake. This gave interesting perspectives to evaluate both growth and maturation and their combined effects on root water uptake. We demonstrated how combinations of different maturation and growth functions lead to different strategies of water uptake.

These solutions were also used to revisit optimal root geometrical parameters for water uptake. Indeed, Landsberg and Fowkes (1978) model had been used to define optimal root systems in terms of water uptake subject to minimal carbon cost (Biondini, 2008). In contrast to their monotonic behaviour of root water uptake capacity with root length, we demonstrated that local root hydraulic conductivity varying with root length lead to very different behaviours. The effective root conductance may increase with root length more steadily than in case of a uniform root or even decrease with root length. Similarly, the maximal water uptake location was no more located at root proximal end. Non-monotonic root water uptake distributions emerged from the new solutions. Therefore, the search for optimal root systems (ideotypes) should not only focus on root architecture or general averaged root hydraulic properties but also account for variations of root properties along roots.

The new models can used to derive local hydraulic properties of roots or be combined as building blocks to generate complete root system hydraulic architectures defining plant genotypes in order to compare plant performances in contrasted environments using soil-plant models such as R-SWMS (Javaux et al., 2008). To do so, it is needed to calculate the macroscopic parameters defined by Couvreur et al. (2012) at the root system scale as a combination of the single root solutions proposed here at the single root scale. This will allow us to simulate plant root system water uptake of varying genotypes over the growing season in contrasted pedo-climatic conditions and hence to look for best genotype by environment interaction.

6 Code availability

The code is available and can be freely shared.

7 Data availability

Not applicable

References

Alm, D. M., Cavelier, J., and Nobel, P. S.: A Finite-element Model of Radial and Axial Conductivities for Individual Roots: Development and Validation for Two Desert Succulents, Annals of Botany, 69, 87–92, 1992.

Ariyaratna, R.: An extension to the Landsberg and Fowkes' Model, Ph.D. thesis, Texas Tech University, https://ttu-ir.tdl.org/ttu-ir/handle/2346/19780, 1990.

Bechmann, M., Schneider, C., Carminati, A., Vetterlein, D., Attinger, S., and Hildebrandt, A.: Effect of parameter choice in root water uptake models – the arrangement of root hydraulic properties within the root architecture affects dynamics and efficiency of root water uptake, Hydrology and Earth System Sciences, 18, 4189–4206, doi:10.5194/hess-18-4189-2014, http://www.hydrol-earth-syst-sci.net/18/4189/2014/, 2014.

Biondini, M.: Allometric scaling laws for water uptake by plant roots, Journal of Theoretical Biology, 251, 35–59, doi:10.1016/j.jtbi.2007.11.018, http://linkinghub.elsevier.com/retrieve/pii/S0022519307005784, 2008.

Bramley, H., Turner, N. C., Turner, D. W., and Tyerman, S. D.: Comparison between gradient-dependent hydraulic conductivities of roots using the root pressure probe: the role of pressure propagations and implications for the relative roles of parallel radial pathways, Plant, Cell & Environment, 30, 861–874, doi:10.1111/j.1365-3040.2007.01678.x, http://doi.wiley.com/10.1111/j.1365-3040.2007.01678.x, 2007.

Campos, H., Cooper, M., Habben, J., Edmeades, G., and Schussler, J.: Improving drought tolerance in maize: a view from industry, Field Crops Research, 90, 19–34, doi:10.1016/j.fcr.2004.07.003, http://www.sciencedirect.com/science/article/pii/S0378429004001571, 2004.

Cattivelli, L., Rizza, F., Badeck, F.-W., Mazzucotelli, E., Mastrangelo, A. M., Francia, E., Marè, C., Tondelli, A., and Stanca, A. M.: Drought tolerance improvement in crop plants: An integrated view from breeding to genomics, Field Crops Research, 105, 1–14, doi:10.1016/j.fcr.2007.07.004, http://www.sciencedirect.com/science/article/pii/S0378429007001414, 2008.

Chaumont, F. and Tyerman, S. D.: Aquaporins: Highly Regulated Channels Controlling Plant Water Relations, PLANT PHYSIOLOGY, 164, 1600–1618, doi:10.1104/pp.113.233791, http://www.plantphysiol.org/cgi/doi/10.1104/pp.113.233791, 2014.

Couvreur, V., Vanderborght, J., and Javaux, M.: A simple three-dimensional macroscopic root water uptake model based on the hydraulic architecture approach, Hydrol. Earth Syst. Sci, 16, 2957–2971, http://www.hydrol-earth-syst-sci-discuss.net/9/4943/2012/hessd-9-4943-2012.pdf, 2012.

Couvreur, V., Vanderborght, J., Beff, L., and Javaux, M.: Horizontal soil water potential heterogeneity: simplifying approaches for crop water dynamics models, Hydrology and Earth System Sciences, 18, 1723–1743, doi:10.5194/hess-18-1723-2014, http://www.hydrol-earth-syst-sci.net/18/1723/2014/, 2014.

Doussan, C., Pagès, L., and Vercambre, G.: Modelling of the Hydraulic Architecture of Root Systems: An Integrated Approach to Water Absorption—Model Description, Annals of Botany, 81, 213–223, doi:10.1006/anbo.1997.0540, http://aob.oxfordjournals.org/cgi/doi/10.1006/anbo.1997.0540, 1998a.

Doussan, C., Vercambre, G., and Pagès, L.: Modelling of the hydraulic architecture of root systems: An integrated approach to water absorption—distribution of axial and radial conductances in maize, Annals of Botany, 81, 225–232, http://aob.oxfordjournals.org/content/81/2/225.short, 1998b.

Enstone, D. E., Peterson, C. A., and Ma, F.: Root Endodermis and Exodermis: Structure, Function, and Responses to the Environment, Journal of Plant Growth Regulation, 21, 335–351, doi:10.1007/s00344-003-0002-2, http://link.springer.com/10.1007/s00344-003-0002-2, 2002.

Frensch, J. and Steudle, E.: Axial and radial hydraulic resistance to roots of maize (Zea mays L.), Plant Physiology, 91, 719–726, http://www.plantphysiol.org/content/91/2/719.short, 1989a.

Frensch, J. and Steudle, E.: Axial and Radial Hydraulic Resistance to Roots of Maize (Zea mays L.) 1, Plant Physiology, 91, 719–726, http://www.ncbi.nlm.nih.gov/pmc/articles/PMC1062061/, 1989b.

Frensch, J., Hsiao, T. C., and Steudle, E.: Water and solute transport along developing maize roots, Planta, 198, 348–355, doi:10.1007/BF00620050, http://link.springer.com/article/10.1007/BF00620050, 1996.

5 Hachez, C., Moshelion, M., Zelazny, E., Cavez, D., and Chaumont, F.: Localization and Quantification of Plasma Membrane Aquaporin Expression in Maize Primary Root: A Clue to Understanding their Role as Cellular Plumbers, Plant Molecular Biology, 62, 305–323, doi:10.1007/s11103-006-9022-1, http://link.springer.com/10.1007/s11103-006-9022-1, 2006.

Javaux, M., Schröder, T., Vanderborght, J., and Vereecken, H.: Use of a three-dimensional detailed modeling approach for predicting root water uptake, Vadose Zone Journal, 7, 1079–1088, http://vzj.geoscienceworld.org/content/7/3/1079.short, 2008.

10 Landsberg, J. J. and Fowkes, N. D.: Water Movement Through Plant Roots, Annals of Botany, 42, 493–508, doi:10.1093/oxfordjournals.aob.a085488, http://aob.oxfordjournals.org/content/42/3/493, 1978.

Leitner, D., Meunier, F., Bodner, G., Javaux, M., and Schnepf, A.: Impact of contrasted maize root traits at flowering on water stress tolerance – A simulation study, Field Crops Research, doi:10.1016/j.fcr.2014.05.009, http://linkinghub.elsevier.com/retrieve/pii/S037842901400135X, 2014.

15 Lobet, G., Couvreur, V., Meunier, F., Javaux, M., and Draye, X.: Plant Water Uptake in Drying Soils, Plant Physiology, doi:10.1104/pp.113.233486, http://www.plantphysiol.org/cgi/doi/10.1104/pp.113.233486, 2014.

McCully, M. E. and Canny, M. J.: Pathways and processes of water and nutrient movement in roots, Plant and Soil, 111, 159–170, doi:10.1007/BF02139932, http://link.springer.com/10.1007/BF02139932, 1988.

McElrone, A. J., Choat, B., Gambetta, G. A., and Brodersen, C. R.: Water Uptake and Transport in Vascular Plants, Nature Education

20 Knowledge, 5, 6, 2013.

Meunier, F., Javaux, M., Couvreur, V., Draye, X., Javaux, M., Vanderborght, J., and Vanderborght, J.: A new model for optimizing the water acquisition of root hydraulic architectures over full crop cycles, pp. 140–149, IEEE, doi:10.1109/FSPMA.2016.7818300, http://ieeexplore.ieee.org/document/7818300/, 2016.

Meunier, F., Couvreur, V., Draye, X., Vanderborght, J., and Javaux, M.: Towards quantitative root hydraulic phenotyping: novel mathematical

25 functions to calculate plant-scale hydraulic parameters from root system functional and structural traits, Journal of Mathematical Biology, doi:10.1007/s00285-017-1111-z, http://link.springer.com/10.1007/s00285-017-1111-z, 2017.

Pagès, L., Vercambre, G., Drouet, J. L., Lecompte, F., Collet, C., and Le Bot, J.: Root Typ: a generic model to depict and analyse the root system architecture, Plant and Soil, 258, 103–119, http://www.springerlink.com/index/R742L256T7142875.pdf, 2004.

Passioura, J. B.: The transport of water from soil to shoot in wheat seedlings, Journal of Experimental Botany, 31, 333–345, http://jxb.

30 oxfordjournals.org/content/31/1/333.short, 1980.

Roose, T. and Schnepf, A.: Mathematical models of plant–soil interaction, Philosophical Transactions of the Royal Society A: Mathematical, Physical and Engineering Sciences, 366, 4597–4611, http://rsta.royalsocietypublishing.org/content/366/1885/4597.abstract, 2008.

Sanderson, J.: Water Uptake by Different Regions of the Barley Root. Pathways of Radial Flow in Relation to Development of the Endodermis, Journal of Experimental Botany, 34, 240–253, doi:10.1093/jxb/34.3.240, http://jxb.oxfordjournals.org/lookup/doi/10.1093/jxb/34.3.

35 240, 1983.

Steudle, E.: Water uptake by roots: effects of water deficit, Journal of Experimental Botany, 51, 1531–1542, doi:10.1093/jexbot/51.350.1531, http://jxb.oxfordjournals.org/content/51/350/1531, 2000.

Steudle, E. and Peterson, C. A.: How does water get through roots?, Journal of Experimental Botany, 49, 775–788, doi:10.1093/jxb/49.322.775, http://jxb.oxfordjournals.org/content/49/322/775, 1998.

Tardieu, F., Simonneau, T., and Parent, B.: Modelling the coordination of the controls of stomatal aperture, transpiration, leaf growth, and abscisic acid: update and extension of the Tardieu-Davies model, Journal of Experimental Botany, 66, 2227–2237, doi:10.1093/jxb/erv039, 2015.

Vadez, V.: Root hydraulics: The forgotten side of roots in drought adaptation, Field Crops Research, doi:10.1016/j.fcr.2014.03.017, http://linkinghub.elsevier.com/retrieve/pii/S0378429014000872, 2014.

Varney, G. T. and Canny, M. J.: Rates of water uptake into the mature root system of maize plants, New Phytologist, 123, 775–786, doi:10.1111/j.1469-8137.1993.tb03789.x, http://doi.wiley.com/10.1111/j.1469-8137.1993.tb03789.x, 1993.

Volpe, V., Marani, M., Albertson, J. D., and Katul, G.: Root controls on water redistribution and carbon uptake in the soil–plant system under current and future climate, Advances in Water Resources, 60, 110–120, doi:10.1016/j.advwatres.2013.07.008, http://www.sciencedirect.com/science/article/pii/S0309170813001231, 2013.

Zarebanadkouki, M., Meunier, F., Couvreur, V., Cesar, J., Javaux, M., and Carminati, A.: Estimation of the hydraulic conductivities of lupine roots by inverse modelling of high-resolution measurements of root water uptake, Annals of Botany, p. mcw154, doi:10.1093/aob/mcw154, http://aob.oxfordjournals.org/lookup/doi/10.1093/aob/mcw154, 2016.

Zhuang, J., Nakayama, K., Yu, G.-R., and Urushisaki, T.: Estimation of root water uptake of maize: an ecophysiological perspective, Field Crops Research, 69, 201–213, http://www.sciencedirect.com/science/article/pii/S0378429000001428, 2001.

Zwieniecki, M. A., Thompson, M. V., and Holbrook, N. M.: Understanding the Hydraulics of Porous Pipes: Tradeoffs Between Water Uptake and Root Length Utilization, Journal of Plant Growth Regulation, 21, 315–323, doi:10.1007/s00344-003-0008-9, http://link.springer.com/10.1007/s00344-003-0008-9, 2002.

Table 1. Local hydraulic properties $k_r(z)$ and $k_x(z)$ for the different cases.

	$\mathbf{k_r(z)}$	$\mathbf{k_x(z)}$
Constant (uniform) root	$k_r(z) = k_{r0}$	$k_x(z) = k_{x0}$
Linear k_r	$k_r(z) = a_0 z + b_0$	$k_x(z) = k_{x0}$
Linear k_x	$k_r(z) = k_{r0}$	$k_x(z) = c_0 z + d_0$
Linear k_r and k_x	$k_r(z) = a_0 z + b_0$	$k_x(z) = c_0 z + d_0$
Exponential k_r	$k_r(z) = \gamma_2 exp(-\beta_2 z)$	$k_x(z) = k_{x0}$
Exponential k_x	$k_r(z) = k_{r0}$	$k_x(z) = \gamma_1 exp(\beta_1 z)$
Exponential k_r and k_x	$k_r(z) = \gamma_2 exp(-\beta_2 z)$	$k_x(z) = \gamma_1 exp(\beta_1 z)$

Table 2. Linearly independent functions f_1 and f_2 solutions of Eq. (4) according to the functions describing local root hydraulic properties shown in Table 1. Parameters are described in Table 3

	$\mathbf{f_1(z)}$	$\mathbf{f_2(z)}$
Constant (uniform) root	$cosh(\tau z)$	$sinh(\tau z)$
Linear k_r	$Ai\left(\dfrac{az+b}{a^{\frac{2}{3}}k_{x0}^{\frac{1}{3}}}\right)$	$Bi\left(\dfrac{az+b}{a^{\frac{2}{3}}k_{x0}^{\frac{1}{3}}}\right)$
Linear k_x	$\sqrt{\dfrac{2}{c}}\,I_0\left(2\sqrt{\dfrac{d+cz}{c^2}}\right)$	$\sqrt{\dfrac{2}{c}}\,K_0\left(2\sqrt{\dfrac{d+cz}{c^2}}\right)$
Linear k_r and k_x	$exp\left(-\dfrac{\sqrt{a}z}{\sqrt{c_0}}\right)M\left(\dfrac{\sqrt{a}c_0^{3/2}+bc_0-ad_0}{2\sqrt{a}c_0^{3/2}},1,\dfrac{2\sqrt{a}(c_0z+d_0)}{c^{3/2}}\right)$	$exp\left(-\dfrac{\sqrt{a}z}{\sqrt{c_0}}\right)U\left(\dfrac{-\sqrt{a}c_0^{3/2}-bc_0+ad_0}{2\sqrt{a}c_0^{3/2}},1,\dfrac{2\sqrt{a}(c_0z+d_0)}{c^{3/2}}\right)$
Exponential k_r	$I_0\left(\dfrac{2\sqrt{\gamma_r exp(-\beta_2 z)}}{\beta2}\right)$	$K_0\left(\dfrac{2\sqrt{\gamma_r exp(-\beta_2 z)}}{\beta2}\right)$
Exponential k_x	$\dfrac{\sqrt{\gamma_x exp(-\beta_1 z)}}{\beta_1}I_1\left(\dfrac{2\sqrt{\gamma_x exp(-\beta_1 z)}}{\beta_1}\right)$	$\dfrac{\sqrt{\gamma_x exp(-\beta_1 z)}}{\beta_1}K_1\left(\dfrac{2\sqrt{\gamma_x exp(-\beta_1 z)}}{\beta_1}\right)$
Exponential k_r and k_x	$\beta^{-\frac{\beta_1}{\beta}}\gamma^{\frac{\beta_1}{2\beta}}(exp(-\beta z))^{\frac{\beta_1}{2\beta}}\Gamma\left(1-\frac{\beta_1}{\beta}\right)I_{-\frac{\beta_1}{\beta}}\left(\dfrac{2\sqrt{exp(-\beta z)\gamma}}{\beta}\right)$	$\beta^{-\frac{\beta_1}{\beta}}\gamma^{\frac{\beta_1}{2\beta}}(exp(-\beta z))^{\frac{\beta_1}{2\beta}}\Gamma\left(1+\frac{\beta_1}{\beta}\right)I_{\frac{\beta_1}{\beta}}\left(\dfrac{2\sqrt{exp(-\beta z)\gamma}}{\beta}\right)$

Ai and Bi are the Airy functions of the first and second kind; M and U, the confluent hypergeometric function of the first and second kind; I_ν and K_ν, the modified Bessel function of the first and second kind of order ν and Γ is the gamma function.

Table 3. Local hydraulic property function parameters, their units, the expression of combined parameters and their corresponding units.

Parameter	Unit	Combined parameter	Unit
k_{r0}	$\mathrm{LT^{-1}P^{-1}}$	$\tau = \sqrt{\frac{2\pi r k_{r0}}{k_{x0}}}$	$\mathrm{L^{-1}}$
k_{x0}	$\mathrm{L^4 T^{-1}P^{-1}}$	$\kappa = \sqrt{2\pi r k_{r0} k_{x0}}$	$\mathrm{L^3 T^{-1}P^{-1}}$
a_0	$\mathrm{T^{-1}P^{-1}}$	$a = 2\pi r a_0$	$\mathrm{LT^{-1}P^{-1}}$
b_0	$\mathrm{LT^{-1}P^{-1}}$	$b = 2\pi r b_0$	$\mathrm{L^2 T^{-1}P^{-1}}$
c_0	$\mathrm{L^3 T^{-1}P^{-1}}$	$c = \frac{c_0}{2\pi r k_{r0}}$	L
d_0	$\mathrm{L^4 T^{-1}P^{-1}}$	$d = \frac{d_0}{2\pi r k_{r0}}$	$\mathrm{L^2}$
γ_1	$\mathrm{L^4 T^{-1}P^{-1}}$	$\gamma_r = \frac{2\pi r \gamma_2}{k_{x0}}$	$\mathrm{L^{-2}}$
γ_2	$\mathrm{LT^{-1}P^{-1}}$	$\gamma_x = \frac{2\pi r k_{r0}}{\gamma_1}$	$\mathrm{L^{-2}}$
β_1	$\mathrm{L^{-1}}$	$\gamma = 2\pi r \frac{\gamma_2}{\gamma_1}$	$\mathrm{L^{-2}}$
β_2	$\mathrm{L^{-1}}$	$\beta = \beta_1 + \beta_2$	$\mathrm{L^{-1}}$

Appendix A: New solutions of the root water flow equation

In this appendix, we provide detailed solutions of the water flow equation when the root hydraulic properties are constant (Landsberg and Fowkes, 1978) or when they vary linearly or exponentially, alone or together along the root axis. These solutions of the water flow equation (4) have been obtained using the symbolic calculation toolbox of Matlab. All solutions are summarized in Table 2.

A1   Constant root hydraulic properties

The solution of the water flow equation in a uniform root has been proposed by Landsberg and Fowkes (1978). We present their methodology and principal results in this section to illustrate with the simplest case how to derive the water flow equation solution and the macroscopic parameters.

The simplest root is made of constant root properties: axial conductance k_{x0} $[\mathrm{L^4 T^{-1} P^{-1}}]$ and radial conductivity k_{r0} $[\mathrm{LT^{-1}P^{-1}}]$:

$$\begin{cases} k_r(z) = k_{r0} \\ k_x(z) = k_{x0} \end{cases}$$

Equation (4) becomes:

$$k_{x0} \frac{d^2 \Psi_x(z)}{dz^2} = 2\pi r k_{r0} \left(\Psi_x(z) - \Psi_{soil} \right)$$

The general solution of this differential equation is given in terms of hyperbolic sinus and cosinus:

$$\Psi_x(z) = \Psi_{soil} + c_1 cosh(\tau z) + c_2 sinh(\tau z) \tag{A1}$$

where we define τ $[\mathrm{L^{-1}}]$:

$$\tau = \sqrt{\frac{2\pi r k_{r0}}{k_{x0}}}$$

Here, the independent functions $f_1(z)$ and $f_2(z)$ are thus $cosh(\tau z)$ and $sinh(\tau z)$.

The coefficients are obtained for the bottom no-flux boundary conditions in case of single stretch root (see Appendix C and particularly Eq. (C1)):

$$\begin{cases} c_1^{nf} = \frac{\Psi_{collar} - \Psi_{soil}}{cosh(\tau l)} \\ c_2^{nf} = 0 \end{cases}$$

Here and in the following, the superscript nf stands for non-flux. Using these coefficients, we find the general solution of the xylem water potential profile:

$$\Psi_x^{nf}(z) = \Psi_{soil} + (\Psi_{collar} - \Psi_{soil}) \frac{cosh(\tau z)}{cosh(\tau l)}$$

The axial flow is then obtained using Eq. (3)

$$J_x^{nf}(z) = -\kappa (\Psi_{collar} - \Psi_{soil}) \frac{sinh(\tau z)}{cosh(\tau l)}$$

And the macroscopic parameters are derived thanks to Eq. (C4)

5 $K_{rs}^{nf}(l) = \kappa tanh(\tau l)$

$$SUD^{nf}(z) = \tau \frac{cosh(\tau z)}{sinh(\tau l)}$$

where tanh is the hyperbolic tangent and $\kappa \, [\mathrm{L}^3\mathrm{T}^{-1}\mathrm{P}^{-1}]$ is the asymptotic root conductance defined by:

$$\kappa = k_{x0}\tau$$

10 For the bottom flux boundary condition (see Eq. (6)), the coefficients are:

$$\begin{cases} c_1 = (\Psi_{proximal,i} - \Psi_{soil}) \left(\frac{\kappa}{\kappa cosh(\tau l_i) + K_{rs,i-1} sinh(\tau l_i)} \right) \\ c_2 = (\Psi_{proximal,i} - \Psi_{soil}) \left(\frac{K_{rs,i-1}}{\kappa cosh(\tau l_i) + K_{rs,i-1} sinh(\tau l_i)} \right) \end{cases}$$

And the solution of the water flow equation in the root becomes:

$$\Psi_x(z) = \Psi_{soil} + (\Psi_{proximal,i} - \Psi_{soil}) \frac{\kappa cosh(\tau z) + K_{rs,i-1} sinh(\tau z)}{\kappa cosh(\tau l_i) + K_{rs,i-1} sinh(\tau l_i)}$$

which leads to the following axial flow:

15 $$J_x(z) = -\kappa (\Psi_{proximal,i} - \Psi_{soil}) \frac{\kappa sinh(\tau z) + K_{rs,i-1} cosh(\tau z)}{\kappa cosh(\tau l_i) + K_{rs,i-1} sinh(\tau l_i)}$$

The macroscopic parameters become:

$$K_{rs,i}(l_i) = \kappa \left(\frac{\kappa sinh(\tau l_i) + K_{rs,i-1} cosh(\tau l_i)}{\kappa cosh(\tau l_i) + K_{rs,i-1} sinh(\tau l_i)} \right)$$

$$SUD_i(z) = \tau \left(\frac{\kappa cosh(\tau z) + K_{rs,i-1} sinh(\tau z)}{\kappa sinh(\tau l_i) + K_{rs,i-1} cosh(\tau l_i)} \right)$$

20 The flux boundary solutions are a generalization of the non-flux solutions as they converge towards the same results as $K_{rs,i-1} \to 0$.

A2 Linear root hydraulic property profiles

In case of roots with linear hydraulic property profiles, different cases are distinguished and are investigated successively.

A2.1 Linear k_r

Equation (4) can be solved with different root linear hydraulic property profiles. Let us consider a constant axial conductance and a radial conductivity varying linearly along the root:

$$\begin{cases} k_r(z) = a_0 z + b_0 \\ k_x(z) = k_{x0} \end{cases}$$

where $a_0\,[\mathrm{T^{-1}P^{-1}}]$ and $b_0\,[\mathrm{LT^{-1}P^{-1}}]$ are shape parameters.
Equation (4) yields:

$$k_{x0}\frac{d^2\Psi_x(z)}{dz^2} = 2\pi r(a_0 z + b_0)(\Psi_x(z) - \Psi_{soil})$$

and can be rewritten as:

$$\frac{d^2\Psi_x(z)}{dz^2} = \frac{(az+b)}{k_{x0}}(\Psi_x(z) - \Psi_{soil})$$

where we have defined:

$$\begin{cases} a = 2\pi r a_0 \\ b = 2\pi r b_0 \end{cases}$$

with $a\,[\mathrm{LT^{-1}P^{-1}}]$ and $b\,[\mathrm{L^2T^{-1}P^{-1}}]$ the revised shape parameters. The general solution of this differential equation is now:

$$\Psi_x(z) = \Psi_{soil} + c_1 Ai\left(\frac{az+b}{a^{\frac{2}{3}}k_{x0}^{\frac{1}{3}}}\right) + c_2 Bi\left(\frac{az+b}{a^{\frac{2}{3}}k_{x0}^{\frac{1}{3}}}\right) \tag{A2}$$

where c_1 and c_2 can anew be obtained using boundary conditions. Ai and Bi are the Airy functions of the first and second kind, respectively. It is worth noting that we obtain a similar solution if the root radius changes linearly along the root while k_x remains constant.

A2.2 Linear k_x

If the root axial conductance varies while the radial conductivity is constant, i.e.:

$$\begin{cases} k_r(z) = k_{r0} \\ k_x(z) = c_0 z + d_0 \end{cases}$$

with $c_0 \, [\mathrm{L^3 T^{-1} P^{-1}}]$ and $d_0 \, [\mathrm{L^4 T^{-1} P^{-1}}]$ the shape parameters, the general water flow Eq. (4) yields:

$$(c_0 z + d_0) \frac{d^2 \Psi_x(z)}{dz^2} + c_0 \frac{d\Psi_x(z)}{dz} = 2\pi r k_{r0} \left(\Psi_x(z) - \Psi_{soil} \right)$$

Again we rewrite the equation as:

5   $$(cz + d) \frac{d^2 \Psi_x(z)}{dz^2} + c \frac{d\Psi_x(z)}{dz} = \left(\Psi_x(z) - \Psi_{soil} \right)$$

with the following definitions of the revised shape parameters:

$$\begin{cases} c = \frac{c_0}{2\pi r k_{r0}} \\ d = \frac{d_0}{2\pi r k_{r0}} \end{cases}$$

The units of c and d are $[\mathrm{L}]$ and $[\mathrm{L}^2]$, respectively. The general solution becomes:

$$\Psi_x(z) = \Psi_{soil} + \sqrt{\frac{2}{c}} \left(c_1 I_0 \left(2\sqrt{\frac{d+cz}{c^2}} \right) + c_2 K_0 \left(2\sqrt{\frac{d+cz}{c^2}} \right) \right) \tag{A3}$$

10   I_ν and K_ν are the modified Bessel function of the first and second kind of order ν ($\nu = 0$, here), respectively.

A2.3   Linear k_r and k_x

We assume now a linear relation between the hydraulic properties and the distance to the tip:

$$\begin{cases} k_r(z) = a_0 z + b_0 \\ k_x(z) = c_0 z + d_0 \end{cases}$$

The water flow equation becomes:

15   $$(c_0 z + d_0) \frac{d^2 \Psi_x(z)}{dz^2} + c_0 \frac{d\Psi_x(z)}{dz} = 2\pi r (a_0 z + b_0) \left(\Psi_x(z) - \Psi_{soil} \right)$$

After rewriting the parameters it yields:

$$(c_0 z + d_0) \frac{d^2 \Psi_x(z)}{dz^2} + c_0 \frac{d\Psi_x(z)}{dz} = (az + b) \left(\Psi_x(z) - \Psi_{soil} \right)$$

with:

$$\begin{cases} a = 2\pi r a_0 \\ b = 2\pi r b_0 \end{cases}$$

This equation has now the general solution:

5    $$\Psi_x(z) = \Psi_{soil} + exp\left(-\frac{\sqrt{a}z}{\sqrt{c_0}}\right)$$

$$\left(c_1 M\left(\frac{\sqrt{a}c_0^{3/2} + bc_0 - ad_0}{2\sqrt{a}c_0^{3/2}}, 1, \frac{2\sqrt{a}(c_0 z + d_0)}{c_0^{3/2}}\right) + c_2 U\left(\frac{-\sqrt{a}c_0^{3/2} - bc_0 + ad_0}{2\sqrt{a}c_0^{3/2}}, 1, \frac{2\sqrt{a}(c_0 z + d_0)}{c_0^{3/2}}\right)\right) \quad \text{(A4)}$$

with M and U the confluent hypergeometric function of the first and second kind, respectively.

A3   Exponential root hydraulic property profiles

Let us finally consider a root whose root hydraulic properties vary exponentially along the root axis:

10    $$\begin{cases} k_x(z) = \gamma_1 exp(\beta_1 z) \\ k_r(z) = \gamma_2 exp(-\beta_2 z) \end{cases}$$

with γ_1 $[\text{L}^4\text{T}^{-1}\text{P}^{-1}]$, β_1 $[\text{L}^{-1}]$, γ_2 $[\text{LT}^{-1}\text{P}^{-1}]$ and β_2 $[\text{L}^{-1}]$ are shape parameters.

The water flow equation becomes:

$$\frac{\partial^2 \Psi_x(z)}{\partial z^2} + \beta_1 \frac{\partial \Psi_x(z)}{\partial z} = \gamma exp(-\beta z)(\Psi_x(z) - \Psi_{soil})$$

with $\gamma = 2\pi r \frac{\gamma_2}{\gamma_1}$ $[\text{L}^{-2}]$ and $\beta = \beta_1 + \beta_2$ $[\text{L}^{-1}]$.

15   Solutions of this differential equation are of type:

$$\Psi_x(z) = \Psi_{soil} + \beta^{-\frac{\beta_1}{\beta}}\gamma^{\frac{\beta_1}{2\beta}}(exp(-\beta z))^{\frac{\beta_1}{2\beta}}$$

$$\left[c_1\Gamma\left(1 - \frac{\beta_1}{\beta}\right)I_{-\frac{\beta_1}{\beta}}\left(\frac{2\sqrt{exp(-\beta z)\gamma}}{\beta}\right) + c_2\Gamma\left(1 + \frac{\beta_1}{\beta}\right)I_{\frac{\beta_1}{\beta}}\left(\frac{2\sqrt{exp(-\beta z)\gamma}}{\beta}\right)\right] \quad \text{(A5)}$$

with Γ the gamma function and I_ν, again, the Bessel function of the first kind.

20   The cases of mixed constant/exponential hydraulic property may be easily solved using the same methodology.

Appendix B: Macroscopic parameters

To calculate the general form of the macroscopic parameters defined as:

$$
\begin{cases}
K_{rs,i} = \dfrac{J_x(l_i)}{\Psi_{soil} - \Psi_x(l_i)} \\[2ex]
SUD_i(z) = \dfrac{q_r(z)}{J_x(l_i)}
\end{cases}
\tag{B1}
$$

we need to combine combining Eq. (3) and (5) with the root stretch boundary conditions (6). The two unknowns, $c_{1,i}$ and
5    $c_{2,i}$, are given, in matrix notation, by:

$$
\begin{bmatrix}
-k_x(l_{i-1})f'_{1,i}(l_{i-1}) & -k_x(l_{i-1})f'_{2,i}(l_{i-1}) \\
f_{1,i}(l_i) & f_{2,i}(l_i)
\end{bmatrix}
\begin{bmatrix}
c_{1,i} \\
c_{2,i}
\end{bmatrix}
=
\begin{bmatrix}
J_{i-1} \\
\Psi_{proximal,i} - \Psi_{soil}
\end{bmatrix}
\tag{B2}
$$

Inverting the system, Eq. (B2) yields:

$$
\begin{cases}
c_{1,i} = \dfrac{k_x(l_{i-1})f'_{2,i}(l_{i-1})(\Psi_{proximal,i}-\Psi_{soil})+f_{2,i}(l_i)J_{i-1}}{k_x(l_{i-1})\big(f'_{2,i}(l_{i-1})f_{1,i}(l_i)-f'_{1,i}(l_{i-1})f_{2,i}(l_i)\big)} \\[3ex]
c_{2,i} = \dfrac{-k_x(l_{i-1})f'_{1,i}(l_{i-1})(\Psi_{proximal,i}-\Psi_{soil})-f_{1,i}(l_i)J_{i-1}}{k_x(l_{i-1})\big(f'_{2,i}(l_{i-1})f_1(l_i)-f'_{1,i}(l_{i-1})f_{2,i}(l_i)\big)}
\end{cases}
\tag{B3}
$$

In homogeneous soil conditions, the proximal flow J_{i-1} may be expressed as the product of the upstream conductance
10   ($K_{rs,i-1}$ root property) by the potential difference between the soil and the proximal xylem water potential of the root stretch:

$$
J_{i-1} = K_{rs,i-1}\left(\Psi_{soil} - \Psi_x(l_{i-1})\right) = -K_{rs,i-1}\left(c_{1,i}f_{1,i}(l_{i-1}) + c_{2,i}f_{2,i}(l_{i-1})\right)
\tag{B4}
$$

Substituting Eq. (B4) in Eq. (B3) for the i$^{\text{th}}$ stretch, we obtain a set of two equations with two unknowns which after solving
for $c_{1,i}$ and $c_{2,i}$ gives:

$$
\begin{cases}
c_{1,i} = \dfrac{(\Psi_{proximal,i}-\Psi_{soil})\big(-K_{rs,i-1}f_{2,i}(l_{i-1})+f'_{2,i}(l_{i-1})k_x(l_{i-1})\big)}{K_{rs,i-1}f_{1,i}(l_{i-1})f_{2,i}(l_i)-K_{rs,i-1}f_{1,i}(l_i)f_{2,i}(l_{i-1})-f'_{1,i}(l_{i-1})f_{2,i}(l_i)k_x(l_{i-1})+f_{1,i}(l_i)f'_{2,i}(l_{i-1})k_x(l_{i-1})} \\[3ex]
c_{2,i} = \dfrac{(\Psi_{proximal,i-1}-\Psi_{soil})\big(K_{rs,i-1}f_{1,i}(l_{i-1})-f'_{1,i}(l_{i-1})k_x(l_{i-1})\big)}{K_{rs,i-1}f_{1,i}(l_{i-1})f_{2,i}(l_i)-K_{rs,i-1}f_{1,i}(l_i)f_{2,i}(l_{i-1})-f'_{1,i}(l_{i-1})f_{2,i}(l_i)k_x(l_{i-1})+f_{1,i}(l_i)f'_{2,i}(l_{i-1})k_x(l_{i-1})}
\end{cases}
\tag{B5}
$$

15   It is important to mention that these coefficients only depend on the properties of the distal stretches to the stretch of interest
and on the effective conductivity that lumps the properties and their spatial variation in all distal stretches. Combining the
coefficients (B5), the definitions of the macroscopic parameters (B1) and the general solutions (5), (2) and (3), the root system
conductance and the standard uptake density after addition of i stretches become:

$$
\begin{cases}
K_{rs,i} = k_x(l_i)\dfrac{\big(-K_{rs,i-1}f_{2,i}(l_{i-1})+f'_{2,i}(l_{i-1})k_x(l_{i-1})\big)f'_{1,i}(l_i)+\big(K_{rs,i-1}f_{1,i}(l_{i-1})-f'_{1,i}(l_{i-1})k_x(l_{i-1})\big)f'_{2,i}(l_i)}{K_{rs,i-1}f_{1,i}(l_{i-1})f_{2,i}(l_i)-K_{rs,i-1}f_{1,i}(l_i)f_{2,i}(l_{i-1})-f'_{1,i}(l_{i-1})f_{2,i}(l_i)k_x(l_{i-1})+f_{1,i}(l_i)f'_{2,i}(l_{i-1})k_x(l_{i-1})} \\[3ex]
SUD_i(z) = \dfrac{2\pi r k_r(z)}{k_x(l_i)}\dfrac{\big(-K_{rs,i-1}f_{2,i}(l_{i-1})+f'_{2,i}(l_{i-1})k_x(l_{i-1})\big)f_{1,i}(z)+\big(K_{rs,i-1}f_{1,i}(l_{i-1})-f'_{1,i}(l_{i-1})k_x(l_{i-1})\big)f_{2,i}(z)}{\big(-K_{rs,i-1}f_{2,i}(l_{i-1})+f'_{2,i}(l_{i-1})k_x(l_{i-1})\big)f'_{1,i}(l_i)+\big(K_{rs,i-1}f_{1,i}(l_{i-1})-f'_{1,i}(l_{i-1})k_x(l_{i-1})\big)f'_{2,i}(l_i)}
\end{cases}
\tag{B6}
$$

Appendix C: Special case of a single-stretched root

If the root system consist in a single stretch, the distal boundary condition is no-flux and the proximal boundary conditions corresponds to the root collar water potential Ψ_{collar} [P]. l_1 is equivalent to l. Mathematically, the boundary conditions become:

$$
\begin{cases}
J_x(0) = 0 \\
\Psi_x(l) = \Psi_{collar}
\end{cases}
\tag{C1}
$$

The boundary conditions (C1) used in case of a root made of a single stretch can be rewritten as:

$$
\begin{bmatrix} -k_x(0)f_1'(0) & -k_x(0)f_2'(0) \\ f_1(l) & f_2(l) \end{bmatrix} \begin{bmatrix} c_1^{nf} \\ c_2^{nf} \end{bmatrix} = \begin{bmatrix} 0 \\ \Psi_{collar} - \Psi_{soil} \end{bmatrix}
\tag{C2}
$$

As in Appendix A, the superscript nf means no-flux bottom boundary condition. It is used when the root is made of only one stretch. Inverting the matrix we obtain the constants:

$$
\begin{cases}
c_1^{nf} = \frac{f_2'(0)(\Psi_{collar}-\Psi_{soil})}{f_2'(0)f_1(l)-f_1'(0)f_2(l)} \\
c_2^{nf} = \frac{-f_1'(0)(\Psi_{collar}-\Psi_{soil})}{f_2'(0)f_1(l)-f_1'(0)f_2(l)}
\end{cases}
\tag{C3}
$$

The 'non-flux' coefficients (C3) are actually a particular case of the 'flux' coefficients (B5) since the latter tend to the former as $K_{rs,i-1} \to 0$ (or $J_{i-1} \to 0$).

The macroscopic parameters of the single-stretch root are finally given by (using the no-flux coefficients (C3) or equivalently evaluating Eq. (B6) with $K_{rs,i-1} = 0$):

$$
\begin{cases}
K_{rs}^{nf} = k_x(l) \left(\frac{f_2'(0)f_1'(l)-f_1'(0)f_2'(l)}{f_2'(0)f_1(l)-f_1'(0)f_2(l)} \right) \\
SUD^{nf}(z) = \frac{2\pi r k_r(z)}{k_x(l)} \left(\frac{f_2'(0)f_1(z)-f_1'(0)f_2(0)}{f_2'(0)f_1'(l)-f_1'(0)f_2'(l)} \right)
\end{cases}
\tag{C4}
$$

Appendix D: Stretch lengths in heterogeneous roots

Let us consider a growing single root with an initial elongation rate v_0 $[\mathrm{LT}^{-1}]$ and a maximal length l_{max} $[\mathrm{L}]$. Its actual elongation rate $v(t)$ $[\mathrm{LT}^{-1}]$ is given, as in Pagès et al. (2004), at any time t $[\mathrm{T}]$ by:

$$v(t) = v_0 exp\left(\frac{-v_0}{l_{max}}t\right) \tag{D1}$$

5 Integrating Eq. (D1) between 0 and time t, we obtain the actual root length l $[\mathrm{L}]$:

$$l(t) = \int_0^t v(t')dt' = l_{max}\left[1 - exp\left(\frac{-v_0}{l_{max}}t\right)\right] \tag{D2}$$

In the case of the root made of one stretch, the root length can be easily substituted by Eq. (D2) to obtain the macroscopic parameters as a function of time instead of root length. If the root is split in distinct stretches, as we substitute l by t, we need to replace the transition positions by transition ages. An equation of the different root stretch lengths $stretch_i(t)$ $[\mathrm{L}]$ is required
10 (we use the indices i to indicate the zones from the tip to the collar, see Fig. 2).

Inverting Eq. (D2), the root age $age(z,t)$ $[\mathrm{T}]$ at any distance z to the root tip z and at any time t yields:

$$age(z,t) = t + \frac{l_{max}}{v_0}ln\left(\frac{z}{l_{max}} + exp\left(\frac{-v_0}{l_{max}}t\right)\right), \forall z \in [0 \; l(t)] \tag{D3}$$

Equation (D3) is then used to derive the macroscopic parameters and the water flow equation solution of a single root as a function of age or when the root hydraulic properties are defined as a function of time instead of as a function of the distance
15 to the tip. We can also calculate the stretch lengths, $stretch_i$. When the root is older than any transition age (called hereafter $age_i[t]$), it is simply the length differences between two successive transition ages. When the root is younger, then either the root zone length is zero (if the young transition age is not reached yet) or growing limited by the total root length:

$$stretch_i(t) = \begin{cases} 0, t < age_i \\ l_{max}\left(1 - exp\left(\frac{-v_0}{l_{max}}(t - age_i)\right)\right), t \geq age_i \text{ and } t \leq age_{i+1} \\ l_{max}\left(exp\left(-\frac{v_0}{l_{max}}(t - age_{i+1})\right) - exp\left(-\frac{v_0}{l_{max}}(t - age_i)\right)\right), t > age_{i+1} \end{cases} \tag{D4}$$

Appendix E: Use of the analytical solutions to verify numerical models

One of the main advantages of analytical solutions is their possible use to verify the accuracy of numerical algorithms. All the developed solutions should be asymptotic solutions provided by numerical algorithms for infinitely small root segments. In fig. E1, we show how we tested the numerical accuracy of Doussan et al. (1998a)'s algorithm for single root with varying hydraulic properties. In the illustrated case, exponential radial and axial hydraulic functions are chosen for a single root that is 10 cm long. The analytical solution is the solid black line, while blue lines are numerical solution for smaller and smaller root segments (darker and darker blue).
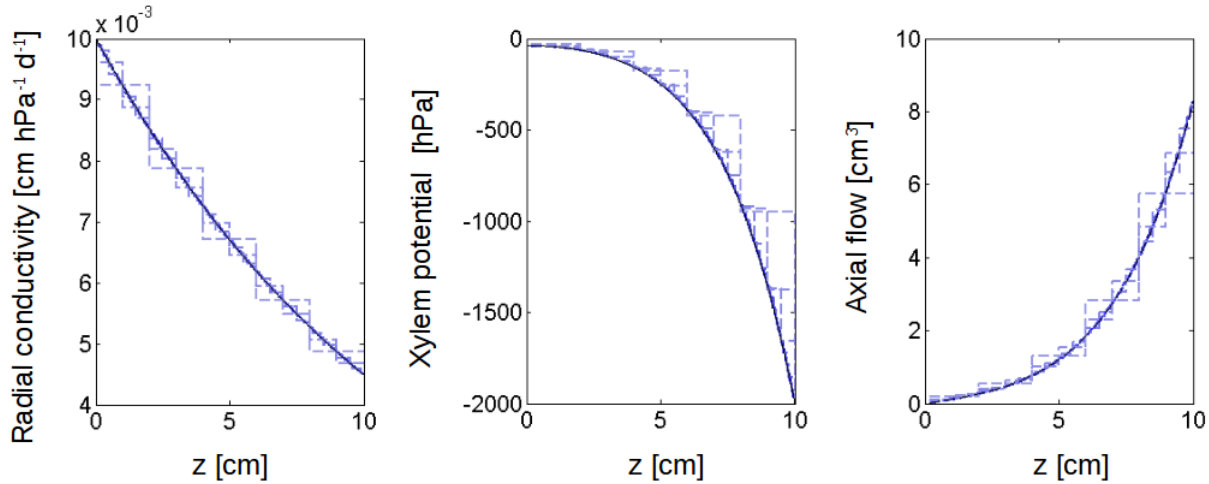
Figure E1. Numerical approximation (blue dashed line) *vs* analytical solution (dark solid line). The smaller the segment size, the better the numerical accuracy.

As the root segment size decreases, the numerical solution tends towards the analytical solution in terms of both xylem potential and axial flow.

Author contributions. F. Meunier solved the water flow equation with the help of V. Couvreur and developed the model used in the simulations. J. Vanderborght, V. Couvreur M. Javaux and X. Draye suggested simulations to illustrate the model and helped in the model conception. M. Zarebanadkouki performed the experiment, treated the data and helped in the analysis of the results. F. Meunier prepared the manuscript with contributions from all co-authors.

5   *Competing interests.* The authors declare that they have no conflict of interest.

Acknowledgements. During the preparation of this manuscript, F. Meunier was supported by the Fonds National de la Recherche Scientifique of Belgium (FNRS) as Research Fellow and is grateful to the organization for its support. This work was also supported by the Belgian French community ARC 16/21-075 project.